Assessment of Isoprene as a Possible Biosignature Gas in Exoplanets with Anoxic Atmospheres

As Published: 10.1089/AST.2019.2146

Publisher: Mary Ann Liebert Inc

Persistent URL: https://hdl.handle.net/1721.1/135597

Version: Final published version: final published article, as it appeared in a journal, conference proceedings, or other formally published context

ASTROBIOLOGY
Volume 21, Number 7, 2021

DOI: 10.1089/ast.2019.2146

Assessment of Isoprene as a Possible Biosignature Gas in Exoplanets with Anoxic Atmospheres

Zhuchang Zhan,[1] Sara Seager,[1–3] Janusz Jurand Petkowski,[1] Clara Sousa-Silva,[1] Sukrit Ranjan,[1] Jingcheng Huang,[4] and William Bains[1,5]

Abstract

The search for possible biosignature gases in habitable exoplanet atmospheres is accelerating, although actual observations are likely years away. This work adds isoprene, C_5H_8, to the roster of biosignature gases. We found that isoprene geochemical formation is highly thermodynamically disfavored and has no known abiotic false positives. The isoprene production rate on Earth rivals that of methane (CH_4; ~500 Tg/year). Unlike methane, on Earth isoprene is rapidly destroyed by oxygen-containing radicals. Although isoprene is predominantly produced by deciduous trees, isoprene production is ubiquitous to a diverse array of evolutionary distant organisms, from bacteria to plants and animals—few, if any, volatile secondary metabolites have a larger evolutionary reach. Although non-photochemical sinks of isoprene may exist, such as degradation of isoprene by life or other high deposition rates, destruction of isoprene in an anoxic atmosphere is mainly driven by photochemistry. Motivated by the concept that isoprene might accumulate in anoxic environments, we model the photochemistry and spectroscopic detection of isoprene in habitable temperature, rocky exoplanet anoxic atmospheres with a variety of atmosphere compositions under different host star ultraviolet fluxes. Limited by an assumed 10 ppm instrument noise floor, habitable atmosphere characterization when using James Webb Space Telescope (JWST) is only achievable with a transit signal similar or larger than that for a super-Earth-sized exoplanet transiting an M dwarf star with an H_2-dominated atmosphere. Unfortunately, isoprene cannot accumulate to detectable abundance without entering a run-away phase, which occurs at a very high production rate, ~100 times the Earth's production rate. In this run-away scenario, isoprene will accumulate to >100 ppm, and its spectral features are detectable with ~20 JWST transits. One caveat is that some isoprene spectral features are hard to distinguish from those of methane and also from other hydrocarbons containing the isoprene substructure. Despite these challenges, isoprene is worth adding to the menu of potential biosignature gases. Key Words: Isoprene—Biosignatures—Anoxic atmospheres—Exoplanets—JWST. Astrobiology 21, 765–792.

1. Introduction

For 90 years, researchers have considered oxygen as a biosignature gas* worth searching for on planets and moons (Jeans, 1930). The upcoming 2021 launch of the James Webb Space Telescope (*JWST*) (Gardner *et al.*, 2006), which will be capable of observing the atmospheres of a handful of prime small rocky exoplanets transiting M dwarf stars, has stimulated the study of potential biosignature gases that could be detected by this and other future space telescope missions.

Beyond JWST, the large ground-based telescopes now under construction (Giant Magellan Telescope, Johns *et al.*, 2012; Extremely Large Telescope, Skidmore *et al.*, 2015; and Thirty Meter Telescope, Tamai and Spyromilio, 2014) are expected to come online in the coming decade, and with the right instrumentation are expected to be able to study rocky planets around M dwarf stars by direct imaging. ESA's Atmospheric Remote-sensing Infrared Exoplanet Large-survey (ARIEL) (Gardner *et al.*, 2006; Pascale *et al.*, 2018) is planned for launch in 2028 and may be able to reach down to observe transiting super-Earth-sized exoplanets around the smallest M dwarf stars. These facilities will provide an excellent opportunity to detect biosignature gases.

However, oxygen alone does not tell the full tale as life on the Earth produces thousands of gases other than oxygen.

*Gases produced by life that accumulate in a planetary atmosphere and are remotely detectable are called ''biosignature gases.''

Departments of [1]Earth, Atmospheric, and Planetary Sciences, [2]Physics, [3]Aeronautics and Astronautics, and [4]Chemistry, MIT, Cambridge, Massachusetts, USA.
[5]Rufus Scientific, Royston, United Kingdom.

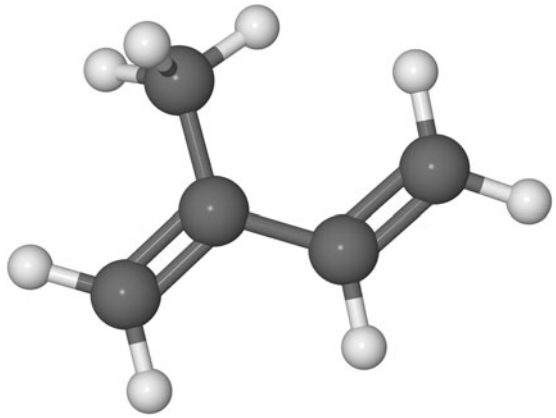

FIG. 1. The chemical structure of isoprene. Carbon atoms are shown in dark gray, and hydrogen atoms are indicated in white. Isoprene (C_5H_8 or 2-methyl-1,3 butadiene) is a conjugated-diene with a methyl group attached to the second position. Conjugated dienes are two double bonds separated by one single bond. C_5H_8, isoprene.

Some volatiles produced by life on the Earth, such as methane (CH_4), and nitrous oxide (N_2O) are prominent in the Earth's atmosphere and therefore have been studied in the context of exoplanet atmosphere biosignature gases. Other gases produced by life are present only as trace gases (<1 parts per billion by volume [ppbv]) in the Earth's atmosphere. The possibility that life elsewhere may generate gases different than gases produced by life on the Earth and in larger quantities has motivated studies of gases such as dimethyl sulfide (DMS), dimethyldisulfide (DMDS), methyl chloride (CH_3Cl), and phosphine (PH_3) (Pilcher, 2003; Segura *et al.*, 2005; Domagal-Goldman *et al.*, 2011; Sousa-Silva *et al.*, 2020). For a review of exoplanet atmosphere biosignature gases, see the works of Grenfell (2018), Kiang *et al.* (2018), Schwieterman *et al.* (2018), and Seager *et al.* (2016).

In this work, we add isoprene (C_5H_8) (Fig. 1) to the list of biosignature gases to be considered for detection in future missions. Isoprene is a hydrocarbon containing two carbon–carbon double bonds connected by one carbon–carbon single bond, or a ''conjugated diene.''

Isoprene on the Earth is predominately produced by deciduous trees and land plants. The production rate of isoprene is about 500 Tg/year (Sharkey *et al.*, 2008), which is comparable to the production rate of methane, also 500 Tg/year (*e.g.*, Dlugokencky *et al.*, 2011). For a more detailed decomposition of isoprene sources and sinks, see Fig. 2. To our knowledge, isoprene has not yet been evaluated in detail as an exoplanet biosignature gas (although it has been briefly mentioned in the works of Seager *et al.*, 2012; Grenfell, 2017).

On first consideration, one might disregard isoprene as a potential biosignature gas because of its short lifetime (<3 hours) in the Earth's atmosphere. The short lifetime results in a very low isoprene atmospheric abundance, ranging from 1 to 5 ppbv only in localized regions above cities and forests (Sharkey *et al.*, 2008) to no detection above deserts. In the Earth's atmosphere, isoprene is primarily regarded as a precursor to secondary organic aerosols. This is because once isoprene is released into the atmosphere it is rapidly destroyed by reactions with •OH,

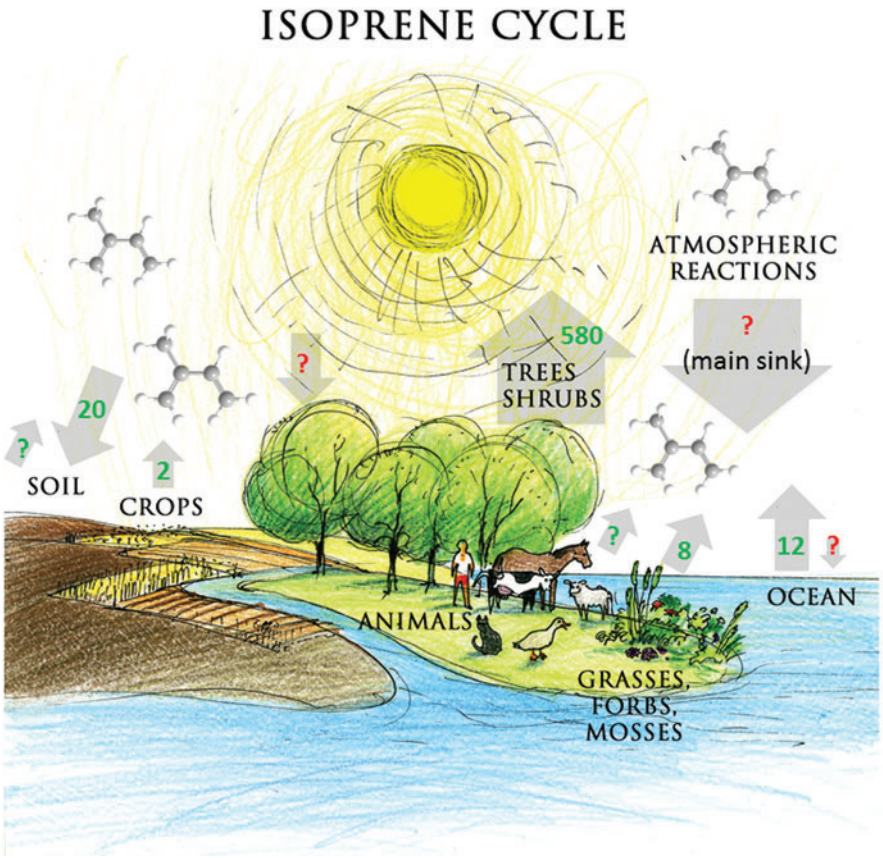

FIG. 2. Schematic of the major sources and sinks of isoprene in the Earth's atmosphere. The isoprene sources (up arrows and green numbers) and sinks (down arrows and red values) are shown. The thickness of arrows provides a relative estimation of the contribution of various sources and sinks of isoprene (McGenity *et al.*, 2018). Color images are available online.

and subsequent reactions with O_2, to form diverse and reactive products. The intermediate products subsequently react with a wide variety of atmospheric components, including trace gases, and NO_3^- and Cl^- radicals, eventually forming aerosols[†] (Fan and Zhang, 2004; Teng *et al.*, 2017) (Fig. 3).

However, the lack of OH^- isoprene under anoxic conditions motivates its assessment as a biosignature gas. The Earth's atmosphere had no oxygen during its initial 2.4 Gyr and isoprene could, in principle, accumulate in anoxic atmospheres to detectable levels (Holland, 2006).

In this article, we evaluate isoprene as a biosignature gas. We first summarize isoprene's sources and sinks (Section 2), including isoprene's overall production on the Earth (Section 2.1), with details on isoprene's biological production from diverse organisms, both aerobic and anaerobic (Section 2.2), followed by a review of the known destruction mechanisms for isoprene (Section 2.3). Next, we outline our inputs and methods to assess the detectability of isoprene for a diverse set of anoxic atmosphere scenarios (Section 3). We discuss our main findings (Section 4): First, we present the production rates required for isoprene to accumulate to a detectable level in a given atmosphere scenario (Section 4.1); next, we assess whether isoprene can be detected by using JWST with a reasonable number of transit observations (Section 4.2); then, we show that isoprene is not produced thermodynamically in the atmosphere and therefore that isoprene as a biosignature gas has no false positives in habitable exoplanet atmospheres (Section 4.3). Finally, we conclude the article with a discussion of our results, limitations, and caveats (Section 5).

2. Isoprene Sources and Sinks

Before we study the detection of isoprene in an exoplanet atmosphere, we first explore how isoprene is created and destroyed. On the Earth, isoprene production is biological (Sections 2.1 and 2.2). We explore the destruction pathways of isoprene, which is mainly by direct photolysis and with OH radicals and O_2 (Fig. 3).

2.1. Isoprene productions on Earth

Globally, life on the Earth produces 400–600 Tg/year of isoprene (Guenther *et al.*, 2006, 2012; Arneth *et al.*, 2008). The biological production rate of isoprene on Earth is roughly equal to global emission of methane from all sources (525 Tg/year) (Guenther *et al.*, 2006, 2012; Seinfeld and Pandis, 2016) and it significantly exceeds production rates of other volatile organic molecules made by life on the Earth such as DMS (38.4 Tg/year), N_2O (20 Tg/year),[‡] and CH_3Cl (3.5 Tg/year) (Fig. 4) (Guenther *et al.*, 2006; Korhonen *et al.*, 2008; Tian *et al.*, 2015; Yokouchi *et al.*, 2015). Isoprene is the most abundantly produced biological volatile organic compound on the Earth and it constitutes more than one-third (by mass) of the total amount of all natural volatile organic compounds released into the Earth's atmosphere (Guenther *et al.*, 2006; Sharkey *et al.*, 2008). For some plants, isoprene can comprise up to 20% of the carbon release rate by the plants (Sharkey and Loreto, 1993). We note that the Earth's isoprene production rate pales in comparison to the production rate of the Earth's most obvious biosignature gas: O_2 (300,000 Tg/year), with one caveat that most of the O_2 is respired and only 0.1% contributes to net O_2 emission (Knoll *et al.*, 2012).

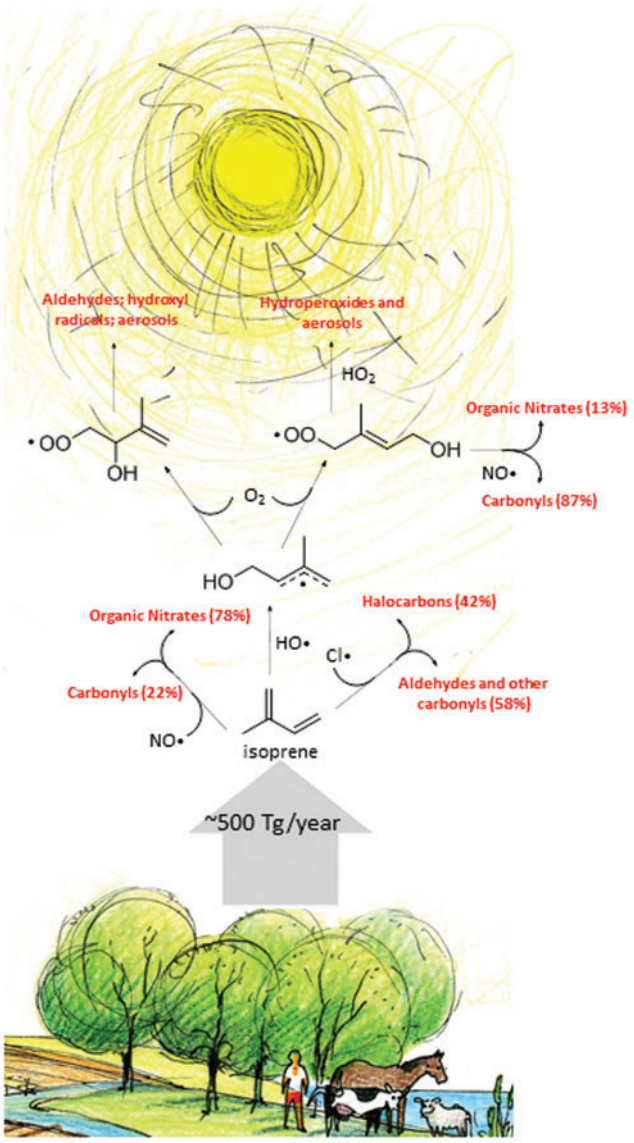

FIG. 3. Schematic of the fate of the isoprene in the Earth's atmosphere. The oxidation of isoprene by OH radicals is the main pathway for the destruction of isoprene in the Earth's atmosphere (Teng *et al.*, 2017). Less predominant destruction pathways include the reaction with NO• and Cl• radicals (Fan and Zhang, 2004). We note that the photochemically driven reactions with minor radical species (*e.g.*, NO• species) can also proceed with downstream isoprene radical products (Iso[O_2]); see, for example, Fan and Zhang (2004) for detailed pathways of photochemically driven atmospheric oxidation of isoprene species. Color images are available online.

[†]For example, the blue haze characteristic of forest-covered mountains (*e.g.*, the Blue Ridge Mountains, a physiographic province of the Appalachian Mountain range) is the end product of isoprene radical chemistry (Claeys *et al.*, 2004).

[‡]With anthropogenic sources the total production of N_2O is 30 Tg/year.

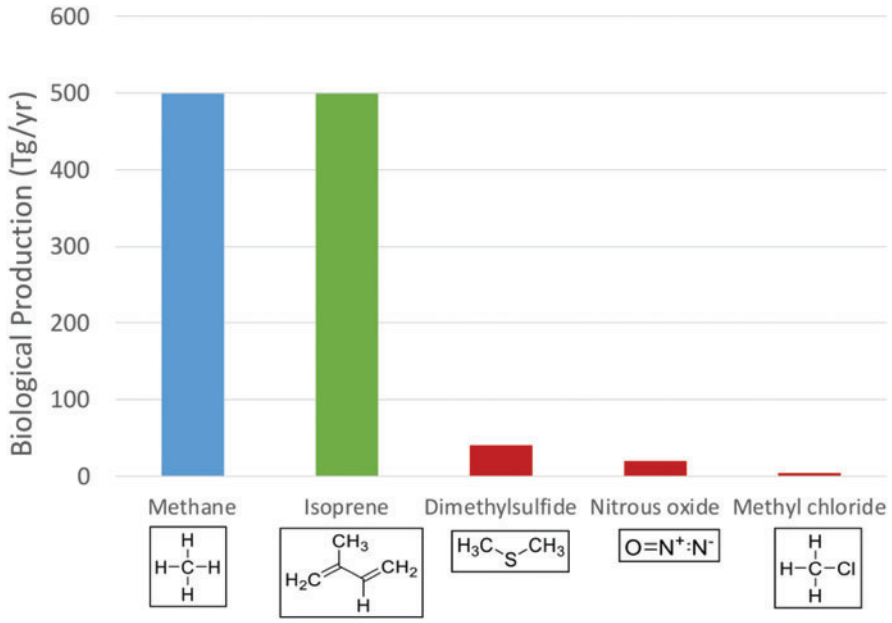

FIG. 4. Estimated biological production of five different gases in Tg/year. Isoprene (green bar) has a production rate in the same range of that of methane (blue bar). Other gases considered as biosignature gases have much lower biological production rates. Data from the following sources: Guenther *et al.* (2006), Korhonen *et al.* (2008), Tian *et al.* (2015), Yokouchi *et al.* (2015). Color images are available online.

Gases such as CH_3Cl (Segura *et al.*, 2005) and DMS (Pilcher, 2003; Domagal-Goldman *et al.*, 2011; Seager *et al.*, 2012; Arney *et al.*, 2018) were suggested earlier as potential biosignature gases due to their large production rate by marine life on Earth and low destruction rate, which lead to relative stability in some atmospheres. Global annual production rates of isoprene are much higher than those of CH_3Cl and DMS (production rates of major volatile secondary metabolites by life on Earth are compared in Fig. 4).

Isoprene has a short atmospheric lifetime of <3 h in the modern terrestrial atmosphere (Section 2.3). The very high destruction rate of isoprene in O_2-dominated environments leads to a very low effective abundance of isoprene in the Earth's atmosphere. Isoprene concentration in the atmosphere varies geographically and seasonally, ranging from 1–5 ppb above forests (Sharkey *et al.*, 2008) to no detection above deserts. However, even in the high-producing areas, above deciduous forests, isoprene concentration does not exceed 5 ppb (Sharkey *et al.*, 2008). Low production rates in other areas means that the global average level of isoprene in the Earth's modern troposphere is less than ppt levels. Such low atmospheric abundances make the remote detection of isoprene in the Earth's atmosphere a challenging task; in fact, isoprene has not been detected in the transmission spectra of the Earth's atmosphere (Schreier *et al.*, 2018), as measured by the ACE-FTS Earth observation mission (Hughes *et al.*, 2014; Bernath, 2017).

2.2. Biological production of isoprene

In this section, we review the biological production of isoprene by life on Earth. We discuss the diversity of species that synthesize isoprene (Section 2.2.1), briefly review isoprene's biosynthesis, explore the production of isoprene by anaerobic life-forms on Earth (Section 2.2.2) and summarize the variety of biological functions of isoprene (Section 2.2.3). We leave an in-depth discussion of the structural and phylogenetic diversity of isoprenoids (isoprene polymers or molecules with isoprene-like structure) and a detailed review of the known isoprenoid biosynthetic pathways for Supplementary Appendix A2.

2.2.1. The extent of formation of isoprene by life on Earth. Isoprene is produced by a very large number of evolutionarily diverse organisms, including algae, animals, bacteria, fungi, plants, and protists (Gelmont *et al.*, 1981; Moore *et al.*, 1994; Kuzma *et al.*, 1995; Sharkey, 1996; Fall and Copley, 2000; Bäck *et al.*, 2010; King *et al.*, 2010; Exton *et al.*, 2013). The majority (~90%) of the global production of isoprene is from terrestrial plants, mostly by tropical trees and shrubs (Sharkey *et al.*, 2008) (see Fig. 2 for an overview of the isoprene cycle in the atmosphere). Animals are responsible for the release of a significant fraction of the remaining 10% of isoprene's yearly global emissions. Production of isoprene was extensively studied in many animal species, but the majority of research was done on isoprene production in rodents and humans (Sharkey, 1996). For example, nursing mice and rats emit substantial amounts of isoprene (Sharkey, 1996). Isoprene is also the most abundant hydrocarbon in the exhaled breath of humans (Gelmont *et al.*, 1981; Sharkey, 1996; King *et al.*, 2010).

In addition to plants and animals, many bacteria, both aerobic and anaerobic, produce isoprene. The true extent of isoprene synthesis in prokaryotes is still difficult to estimate, as only a few phyla have been tested for isoprene production (*e.g.*, Proteobacteria, Actinobacteria, and Firmicutes) (Kuzma *et al.*, 1995; Schöller *et al.*, 1997, 2002; Fall and Copley, 2000; Alvarez *et al.*, 2009). Bacteria from the genus *Bacillus*, both terrestrial and marine, were shown to be the highest producers of isoprene among tested prokaryotes (Kuzma *et al.*, 1995; McGenity *et al.*, 2018). Some *Bacillus* species are also the only bacteria known so far to naturally produce isoprene completely anaerobically (see Section 2.2.2) (Fall *et al.*, 1998).

The endogenous production of isoprene in archaea has not been widely investigated, and isoprene has not yet been found to be produced by archaea.

In summary, isoprene production on the Earth is not only abundant but also widespread and present in a large number of evolutionarily diverse organisms, from bacteria to mammals, and is made by at least two, evolutionarily distinct metabolic pathways (Supplementary Appendix A2). No other volatile secondary metabolite has a larger evolutionary reach than isoprene.

2.2.2. Biosynthesis of isoprene. Isoprene biosynthesis has only been extensively studied in plants. In plants, isoprene synthase (IspS; PDB ID: 3n0g; EC 4.2.3.27) is responsible for the catalysis of the last step in the isoprene biosynthesis pathway—the elimination of pyrophosphate from the isoprene precursor dimethylallyl pyrophosphate (DMAPP) and the release of isoprene (Fig. 5) (Köksal *et al.*, 2010).

The mechanisms of biosynthesis of isoprene in non-plant species are largely unknown despite confirmed widespread isoprene production by a diverse host of organisms. Early studies suggested that mammals synthesize isoprene in the liver through a different pathway than plants (Deneris *et al.*, 1985; Sharkey, 1996). For more detail, see Supplementary Appendix A2.

Interestingly, despite plentiful evidence for bacterial production of isoprene, bacterial isoprene synthase has been only partially characterized and is believed to be evolutionarily unrelated to the plant isoprene synthase (Sivy *et al.*, 2002; McGenity *et al.*, 2018). Isoprene production has been detected in fungi (Berenguer *et al.*, 1991) and animals even if they too, like bacteria, do not seem to have plant isoprene synthase homologs. We conducted a bioinformatic search of genomic databases for sequences similar to plant isoprene synthase sequences and confirmed that no homologues of plant isoprene synthase have been found in bacteria, archaea, fungi, or animals. This confirms that isoprene synthetic pathways have evolved independently at least twice.

Impressively, all species belonging to the three domains of life (Bacteria, Archaea, and Eukarya) possess isoprenoid biosynthetic pathways. This means that all species are capable of producing complicated natural compounds containing the isoprene ''motif,'' even though not all species release isoprene as an isolated molecule (Supplementary Appendix Table A1) (Firn, 2010). For details on isoprenoid biosynthetic pathways, see Supplementary Appendix A2.

Although on Earth life that produces isoprene is aerobic (O_2-dependent) or facultatively anaerobic (*e.g.*, *Escherichia coli* or *Bacillus subtilis*), the biosynthesis of isoprene does not require molecular oxygen (unlike, *e.g.*, the biosynthesis of sterols). This means that isoprene could be, in principle, made by strictly anaerobic organisms, in anoxic atmospheres. The synthesis of isoprene by recombinant anaerobic bacteria and archaea is known (Beck *et al.*, 2014; Murphy *et al.*, 2017). For example, the methanogenic and anaerobic archaea *Methanosarcina acetivorans* is capable of efficient isoprene production on heterologous expression of isoprene synthase from plants (Murphy *et al.*, 2017). There are also a small number of studies of native anaerobic isoprene production in natural environments. A few anaerobic bacteria, such as *Bacillus cereus* 6A1 and *Bacillus lichenformis* 5A24, have been shown to naturally produce isoprene anaerobically, and in substantial quantities, with production rates of 40–60 nmol/(g·hour) (Fall *et al.*, 1998), comparable to that of terrestrial plants as demonstrated in Section 4.1.2, where we discuss in detail the global production rate achievable for an Archean anoxic biosphere comprising purely isoprene-producing prokaryotes.

Indeed, the capability for isoprene biosynthesis appears to be independent of aerobic metabolism. Such few laboratory studies on anaerobic production of isoprene establish the precedent that alien life could, in principle, discover an anaerobic biosynthetic pathway to produce isoprene, even on planets that have atmospheres very different than the Earth's (*e.g.*, H_2-dominated). We note that H_2-dominated atmospheres are not detrimental for life and that life can survive and actively reproduce in an H_2-dominated environment (Seager *et al.*, 2020). There is, however, the question of sufficient evolutionary incentive for production of huge amounts of isoprene by an anaerobic biosphere. We discuss this problem next.

The reasons that the Earth's aerobic biosphere makes isoprene in such impressively large amounts is not known, and it is not yet known what are the evolutionary pressures that govern isoprene production by life on the Earth (Sharkey and Monson, 2017). It is, however, likely that the functions of isoprene for life on Earth are many and are not limited to one single dominant role (see Section 2.2.3 below for discussion of various biological functions of isoprene). The biological functions of isoprene may be related to ultraviolet (UV) shielding and reactive-UV-radical protection (as evidenced by plants' response to UV, heat etc.); isoprene might also be used as a signaling molecule (Harvey and Sharkey, 2016; Zuo *et al.*, 2019). It is impossible to predict what biological functions a specialized secondary metabolite such as isoprene could have in an anaerobic setting. One could speculate that the protective role of isoprene against UV radiation and/or other stressors could be universal to all life, even an anaerobic one, and therefore could justify its abundant production in an anoxic world, especially as the anoxic world would have no ozone layer to protect against UV.

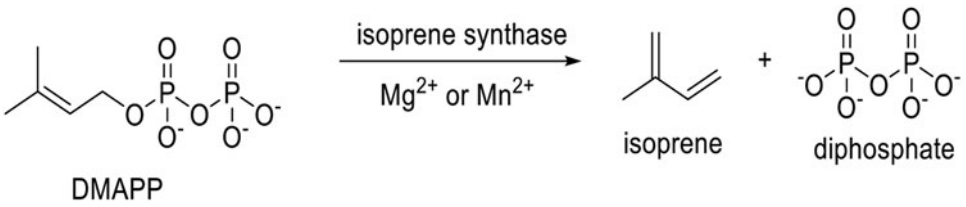

FIG. 5. Biological production of isoprene. Isoprene synthase is an Mg^{2+}- or Mn^{2+}- dependent terpenoid synthase that catalyzes the cleavage of inorganic diphosphate from the isoprene precursor DMAPP to yield isoprene. DMAPP, dimethylallyl diphosphate.

It is likely that more endogenous isoprene production among archaea and other anaerobic organisms awaits discovery. We hope that this article stimulates further research into this understudied aspect of isoprene biology.

2.2.3. Biological functions of isoprene. The biological roles of isoprene have mostly been studied in plants, as plants are responsible for more than 90% of isoprene production on the Earth. The consensus is that isoprene protects the photosynthetic apparatus of tree leaves from heat stress, especially the sudden changes in temperature caused by varying exposure to sunlight (Sharkey *et al.*, 2008), although other functions have been proposed (Laothawornkitkul *et al.*, 2008; Vickers *et al.*, 2009; Velikova *et al.*, 2012; Jones *et al.*, 2016; Sharkey and Monson, 2017). A range of observations supports this thermal protection role for isoprene (Logan *et al.*, 2000; Peñuelas *et al.*, 2005; Taylor *et al.*, 2019), although its mechanism of action is not known.

The function of isoprene in bacteria, fungi, or animals is far less studied than its function in plants. In a facultative anaerobe bacterium *B. subtilis*, isoprene synthesis is elevated as a response to hydrogen peroxide treatment (Xue and Ahring, 2011; Hess *et al.*, 2013) or in response to nonoptimal growth conditions (*e.g.*, elevated temperature and salinity) (Xue and Ahring, 2011). It has also been suggested that isoprene might play a role as a signaling molecule in the regulation of spore development of *B. subtilis* (Wagner *et al.*, 1999; Fall and Copley, 2000; Sivy *et al.*, 2002). The role of isoprene as an interspecies signaling molecule was also postulated. Isoprene could also act as a repellant for microbe-grazing springtails (hexapods) (Michelozzi *et al.*, 1997; Fall and Copley, 2000; Gershenzon, 2008). Despite the fact that animals produce significant amounts of isoprene, our knowledge of its biological function in animals is still limited.

2.3. Isoprene atmospheric chemistry

Here, we list the dominant known pathways for isoprene loss in the atmosphere. Isoprene is not known to reform from any of its reaction products by any known atmospheric processes, unlike other atmospheric gases such as H_2O or O_2. Isoprene has very low water solubility, so isoprene itself is not likely to be absorbed into an aerosol or rained out, though we do model this process. We, therefore, consider the source of isoprene to be solely biological production, and the main sink of isoprene to be photochemistry.

In the Earth's atmosphere, isoprene's main destruction pathways are: (1) direct photolysis and (2) reaction with •OH radicals and these are subsequently followed by reaction with O_2. Isoprene also reacts with other radicals but their abundance is too low compared with •OH radicals to make a significant impact (Fan and Zhang, 2004). However, there might be as yet unknown isoprene destruction pathways in anoxic atmospheres that might affect the overall destruction rate of isoprene significantly. Directed experimental studies, for example, similar to that of He *et al.* (2019) on the chemistry of isoprene in different atmospheric scenarios (especially anoxic ones), are needed to fully understand the scope of isoprene's possible reactions in diverse exoplanet atmospheres.

The reaction rate constants used in the following subsections are constants in the Arrhenius rate equation: $k = Ae^{-E/RT}$, where k is the reaction rate constant (cm^3/s for a second-order reaction), A is a constant (cm^3/s), E is the activation energy (J/mol), R is the gas constant [J/(mol·K)], and T is temperature (K).

2.3.1. Destruction by •OH radicals and O_2. Isoprene's reaction with •OH is the first step in a series of reactions that end with aerosol formation (Fig. 6) (*e.g.*, Zhang *et al.*, 2000). The rate coefficient for the destruction of isoprene by reaction with •OH is $k = 10.0 \pm 1.2 \times 10^{-11}$ cm^3/(molecule·s) at 294 K (Zhang *et al.*, 2000). The •OH radical can attack different positions of the isoprene molecule to create intermediate sets of radicals with the general formula:

$$C_5H_8 + \cdot OH \rightarrow \cdot C_5H_8[OH] \quad (1)$$

In an anoxic atmosphere, •OH will still be present (from H_2O photodissociation) but at much lower levels than in an

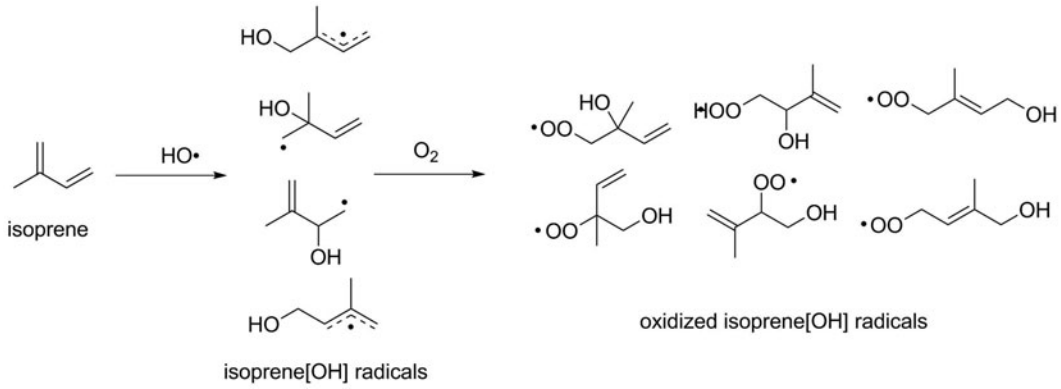

FIG. 6. A mechanistic diagram for the reactions of •OH with isoprene and the subsequent •C_5H_8[OH] radical reactions with O_2. The dots indicate the location of the radicals. The dashed lines indicate the delocalized electrons. The four isoprene intermediates (left side) immediately react with O_2, resulting in six different radicals (right side). The six radicals react with other trace atmospheric components to form aerosols. Figure adapted from the work of Zhang *et al.* (2000).

oxygenic atmosphere (Hu *et al.*, 2012). Therefore, the fate of $^{\bullet}C_5H_8[OH]$ radicals, in the absence of oxygen, will depend on the trace constituents of a given atmosphere. To our knowledge, the reaction network for $^{\bullet}$C5H8[OH] is not known for anoxic conditions; therefore, as with the other products of isoprene destruction, we neglect its chemistry to focus on the prospects for isoprene buildup, with the understanding that this approximation may lead to underestimates of the isoprene concentration at a given isoprene surface flux since we neglect the possibility of isoprene recombination and/or UV shielding from isoprene photochemical products.

In the Earth's atmosphere, the intermediate $^{\bullet}C_5H_8[OH]$ radicals then react with O_2. The product oxidized isoprene radicals ($^{\bullet}C_5H_8[OH][O_2]$) subsequently react with $NO_x^{\bullet}$ species in the atmosphere and other reactive trace gases, contributing to the overall destruction rate of isoprene (Zhang *et al.*, 2000; Fan and Zhang, 2004). We ignore the subsequent reactions of isoprene radicals for anoxic atmospheres where oxygen is not present.

2.3.2. Destruction by O_3. Isoprene can react directly with O_3 with the rate coefficient $k = 9.6 \pm 0.7 \times 10^{-18}$ cm^3/(molecule·s) at 286 K (Karl *et al.*, 2004). We include the destruction rate of isoprene by O_3 for completeness; the reaction rate is several orders of magnitude smaller than the dominant pathways (reaction with $\cdot$OH, O$^{\bullet}$).

2.3.3. Destruction by O$^{\bullet}$ radicals. Isoprene can react directly with O$^{\bullet}$ with the rate coefficient $k = 3.5 \pm 0.6 \times 10^{-11}$ cm^3/(molecule·s) at 298 K (Paulson *et al.*, 1992).

2.3.4. Destruction by H$^{\bullet}$ radicals and H_2 molecules. To our knowledge, there are no data published on the reactivity of isoprene with hydrogen (H$^{\bullet}$) radicals. Although there are plenty of documented reactions of H$^{\bullet}$ radicals with ethene, propene, and butene (Linstrom and Mallard, 2001), it is beyond the scope of this work to extrapolate from these reactions to isoprene. Further experimental work is needed to confirm or rule out the possibility of efficient conversion of isoprene with H$^{\bullet}$ radicals in H_2-dominated conditions. It is also not known whether any of the $^{\bullet}C_5H_8[OH]$ radicals, formed on reacting with $\cdot$OH, can efficiently react with H$^{\bullet}$ radicals in an H_2-dominated environment to revert back to isoprene and water.

Hydrogenation of isoprene (or isoprene units) by using molecular hydrogen, which results in saturation of a double bond, is a standard reaction used in human industry. However, such reactions require higher than habitable temperatures (>400 K), catalysts and meticulous environments (Abdelrahman *et al.*, 2017). It is also unknown whether lightning might be a catalyst for such reactions to occur in the atmosphere.

2.3.5. Destruction through UV radiation. The general chemical formula for photodissociation of isoprene is:

$$C_5H_8 + h\nu(\lambda_{peak} \cong 218 \text{ nm}) \rightarrow \ \cdot C_5H_7^{-} + H^{+}, \qquad (2)$$

where $h\nu$ is the energy of a photon. To the best of our knowledge, the quantum yield of isoprene photolysis is also not well known. We take a conservative approach and assume the quantum yield of 1, which means that any high-energy UV photon that is absorbed by an isoprene molecule will dissociate it.[§]

2.3.6. Destruction by life. Apart from the atmospheric sinks of $\cdot$OH, O_2, and UV photolysis, $\sim$4% (20 Tg/year) of the yearly production of isoprene is directly consumed as a carbon source by a variety of soil microorganisms (Cleveland and Yavitt, 1998; Shennan, 2005). Although on Earth the biological sink of isoprene is small, it may be reasonable to assume that any atmosphere that is enriched with isoprene will have a sizable population of living organisms utilizing isoprene as a carbon source, further contributing to its removal from the atmosphere. The efficiency of biologically driven removal of isoprene will be largely dependent on the unique biochemistry and ecology of life inhabiting the planet. The impact of the potential biological destruction of isoprene has, therefore, not been included in our model.

2.3.7. Aerosol and haze formation. On Earth, isoprene radical-induced aerosols are a major source of secondary organic aerosols. The production of haze is also the primary pathway for isoprene destruction on the Earth (*e.g.*, Seinfeld and Pandis, 2016). For example, the blue haze of some forest-covered mountains (Claeys *et al.*, 2004) is a product of isoprene radical-induced aerosols.

In the context of anoxic atmospheres, hazes and aerosols would be different from those found in the Earth's atmosphere, with haze composition depending on the molecules and radicals available to react with isoprene and isoprene's destruction products.

3. Inputs and Methods for the Assessment of Detectability

The goal of this section is to provide a framework to assess whether or not a biosignature gas may be detectable given a proposed exoplanet atmospheric context and the reality of telescope observations. Our ability to detect a biosignature gas depends on the dominant molecular composition of the exoplanet atmosphere, observatory capabilities, and instrumental effects. Whether or not a biosignature gas is detectable seldom has a simple, fixed answer.

We start with addressing isoprene molecular absorption inputs, including UV cross-sections used in the photochemistry calculations, infrared (IR) cross-sections used in calculating molecular absorption, and haze extinction cross-sections (Section 3.1). Next, we describe the photochemistry code used to compute the mixing ratio profile used for each atmosphere archetype (Section 3.2) and additional parameters to compute atmospheric simulations (Section 3.3). Then, we describe the simulation of transmission spectroscopy and secondary eclipse thermal emission spectroscopy

[§]We note that the conjugated diene structure of isoprene stabilizes the radical formed by photolysis so that lower energy photons can cleave the C-H bond. The conjugated diene also has a high cross-section for the absorption of UV photons. These two features mean that conjugated dienes such as isoprene are photolyzed with higher efficiency compared with other hydrocarbons.

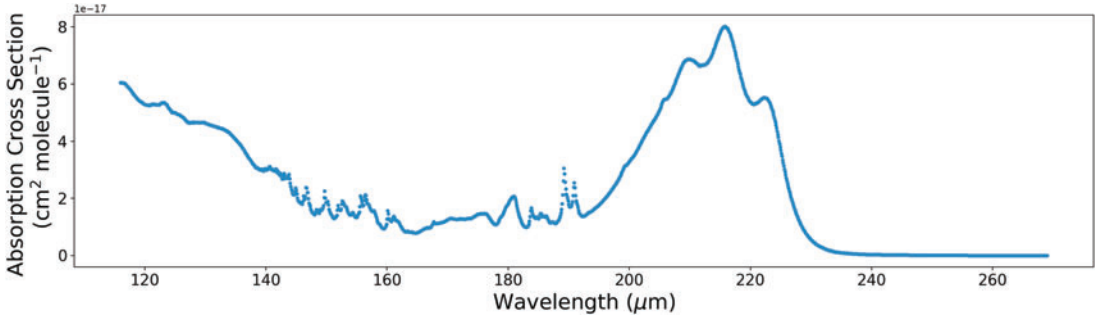

FIG. 7. Isoprene UV-Vis absorption cross-section taken from (Dillon *et al.*, 2017). The axes show absorption cross-section (cm^2/molecule) versus wavelength (μm). The peak absorption of isoprene UV-Vis is at 218 nm. UV-Vis, ultraviolet-visible. Color images are available online.

(Section 3.4). Finally, we discuss observation strategies (Section 3.5) and describe the framework to assess the detection of isoprene (Section 3.6).

3.1. Isoprene molecular inputs

Molecular absorption cross-sections of isoprene are required for calculating the photochemistry rate in the ultraviolet-visible (UV-Vis) regime and simulating its absorption spectral features in an exoplanet atmosphere in the IR regime.

3.1.1. UV-Vis cross-section. The isoprene UV-Vis cross-section is shown in Fig. 7. The data have been taken from Dillon *et al.* (2017) and are used for calculating the UV photolysis rate (see Section 3.3). The isoprene UV-Vis absorption peaks at 218 nm with $\sigma_{peak} = 7.93 \pm 0.02 \times 10^{-17}$/($cm^2$/molecule) and covers a wavelength range of 118–278 nm.

3.1.2. IR cross-sections and uncertainty estimates. The isoprene IR absorption cross-sections are shown in Fig. 8. The data are measured by Brauer *et al.* (2014) and are collected and calibrated by the ''HITRAN online Absorption Cross Sections Database'' (Gordon *et al.*, 2017).

The isoprene cross-section datasets are measured at standard pressure for 278 K, 298 K, and 323 K with a 1/8 cm^{-1} resolution. In this study, we opt to only use the 298 K data to assess the detectability of isoprene because it has the least uncertainties. More specifically, measurements at standard pressure and temperature do not require heating/cooling of the experimental setup, and will, therefore, have the least variation between the source and background reference spectra. As a side note, the methodology for the consideration of the noise floor differs between the 298 K data and the 278 K/323 K data. As a result of this difference in treatment, it is not possible to reliably extrapolate the measured cross-sections to temperatures beyond those

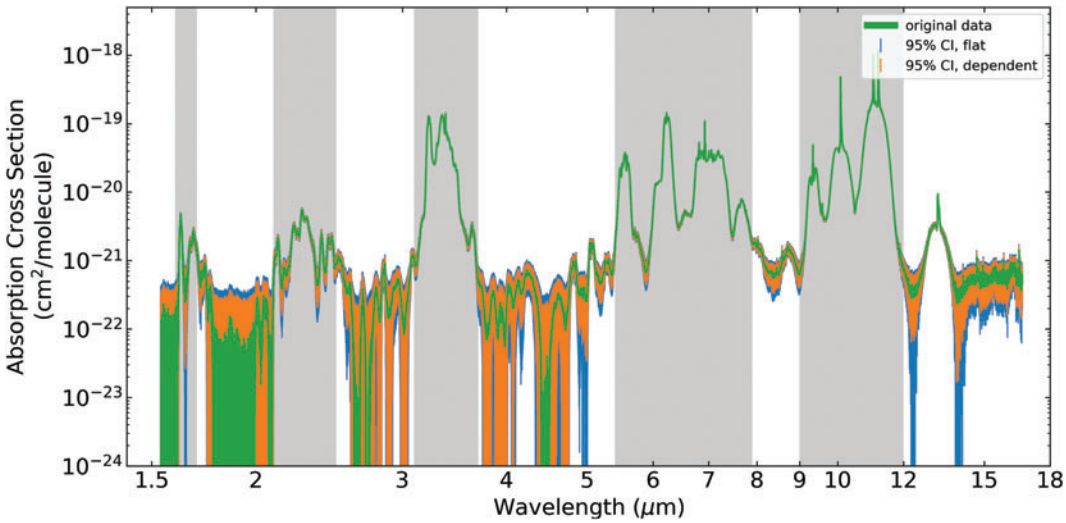

FIG. 8. Isoprene high-resolution IR cross-sections at standard pressure and temperature in log-log scale from 1.3 to 18 μm. Shown in green are isoprene cross-sections, as collected by Brauer *et al.* (2014) and calibrated by HITRAN (Gordon *et al.*, 2017). Shown in blue are the isoprene cross-sections with a uniform uncertainty of 3×10^{-22} cm^2/molecule. Shown in orange is the estimated wavelength-dependent uncertainty based on methods described in the work of Chu *et al.* (1999). The uncertainties represent the 95% confidence interval of the data. Marked in gray are the five regions of isoprene spectral features that we consider to evaluate the detectability of isoprene (1.6–1.7, 2.1–2.5, 3.1–3.7, 5.4–7.9 and 9–12 μm). We omit assessment of the spectral features in other regions due to high uncertainties and omit features longer than 12 μm due to high instrumental noise from the JWST MIRI LRS Instrument (Batalha *et al.*, 2017). IR, infrared; JWST, James Webb Space Telescope. Color images are available online.

measured. Including all three measurements with different noise floor treatments may introduce additional uncertainties to our models.

Unlike absorption cross-sections calculated from molecular line lists, the uncertainties of absorption cross-sections calculated from lab-measured transmission spectra cannot be ignored, especially for data points with opacities that approach the instrument noise floor.

We estimated the wavelength-dependent uncertainties (95% confidence interval of the measured data) as described in Eq. 4 in the work of Chu *et al.* (1999) as follows:

$$\boldsymbol{U \approx 2 \cdot \left(Ba^2 + Ca + D\right)^{\frac{1}{2}}} \quad (3)$$

where U is the expanded uncertainty, a is the absorption-cross section, and B, C, and D are coefficients unique for each molecule. The uncertainty U is the 95% confidence interval. We compare the wavelength-dependent uncertainties with a uniform 3×10^{-22} cm^2/molecule noise floor, as described in the work of Brauer *et al.* (2014) and approximately validate this method by finding the same averaged value. Therefore, both methods are sufficient to identify which data points we can trust and which may be no different than noise, but in general, the uncertainty of the wavelength-dependent method scales with the cross-section values (uncertainties for the largest peaks are larger than the uniformed uncertainty, and uncertainties for the small peaks near the noise floor are smaller than the uniformed uncertainty).

We note that the specific values of the B, C, and D coefficients for isoprene are not measured by Chu *et al.* (1999); they are not provided in the original work of Brauer *et al.* (2014) and are also missing in the NIST spectral database (Linstrom and Mallard, 2001). We, therefore, adopt the values of $B=1.6\times10^{-4}$, $C=1.1\times10^{-9}$, $D=2.7\times10^{-14}$ from C_4H_6 (1-3-butadiene). Although we expect this substitution to introduce some additional uncertainty, it is the most appropriate approximation; C_4H_6 is structurally similar to isoprene (2-Methyl-1,3-butadiene), though it has one less methyl group.

3.1.3. Isoprene spectral features. Isoprene has 33 fundamental IR-active vibrational modes, associated with several functional groups containing carbon–carbon and carbon–hydrogen bonds. The fundamental vibrational modes of isoprene have previously been assigned from both measured and theoretically calculated spectra (Panchenko and De Maré, 2008; Brauer *et al.*, 2014).

We assess the detectability of isoprene in the context of JWST's observation capabilities (see Sections 3.4 and 4.2). We have divided the isoprene spectral features into five wavelength regions: 1.6–1.7, 2.1–2.5, 3.1–3.7, 5.4–7.9, and 9–12 μm. We omitted spectral features in other regions due to the high measurement error-bars and omitted spectral features above 12 μm due to the high instrumental noise of JWST Mid-Infrared Instrument Low-resolution Spectrometer beyond 12 μm (Batalha *et al.*, 2017).

Isoprene cross-section features in the 1.6–1.7 and 2.1–2.5 μm regions are formed by rovibrational overtones of the 3.1–3.7 μm region bands. Features in these two regions lack reliable experimental measurements (Brauer *et al.*, 2014), and detectability of these two spectral features should be taken with some caution. This article motivates future measurements and theoretical simulations of isoprene spectra in the visible and near-IR, as it would expand the assessment of isoprene detection by using more readily available instruments that cover these spectral regions.

Isoprene spectral features in the 3.1–3.7 μm region primarily comprise the following two features: (1) the narrow bands around 3.2 μm, which are composed of the ν_1 and ν_2 asymmetric stretching modes; (2) the broader bands (3.3–3.7 μm), which are composed of the ν_3 (symmetric stretch), ν_4 (asymmetric stretch), and ν_{24} (deformation) modes (Brauer *et al.*, 2014). These two features arise from the stretching modes of X=C-H (sp^2 hybridized) and X-C-H (sp^3 hybridized), where X denotes another atom (other than H).

Isoprene spectral features in the 5.4–7.9 μm region comprise the following two features: (1) the narrow features around 6.5 μm, which are composed of the symmetric and asymmetric stretching modes (ν_8 and ν_9) associated with the C=C double bond; (2) the features in the 6.6–7.9 μm region that are composed of the ν_{10-13} and ν_{24} modes associated with deformation and scissoring rovibrational motions (Brauer *et al.*, 2014).

Isoprene spectral features in the 9–12 μm region comprise several bands associated with the wagging modes of the carbon–hydrogen functional groups (ν_{26}, ν_{27}, and ν_{28}), and one associated with the rocking motion of the X=C-H functional group (ν_{17} mode) (Brauer *et al.*, 2014).

3.1.4. Haze extinction cross-section. We anticipate that abundance of isoprene, a hydrocarbon, in an atmosphere could lead to the presence of a haze layer in the atmosphere similar to the haze layer induced by organic molecules described in the work of Arney *et al.* (2018). The presence of a haze layer may hinder detection of isoprene spectral features and should be quantified.

Studying the effects of isoprene-induced haze requires wavelength-dependent refractive indices and haze particle size distribution, but neither is available for isoprene as studies regarding reactions of the isoprene-induced radicals (or products of isoprene reactions described in Section 2.3) are limited. Isoprene-induced haze on the Earth does not have measurements in IR thus far, and in any case, the Earth's isoprene-induced haze is an oxygenated product not likely to be the same as the isoprene-induced haze on an anoxic exoplanet. Therefore, we estimate the isoprene-induced haze extinction cross-section by using wavelength-dependent refractive index measurements and haze particle-size distributions of other hydrocarbons in a reducing environment.

We adopt the wavelength-dependent refractive indices of Titan's methane-induced haze (measured by Khare *et al.*, 1984), or tholins, as a proxy for that of isoprene-induced hazes. In our solar system, Titan (Khare *et al.*, 1984), Pluto (Zhang *et al.*, 2017), and Venus have extensive haze layers in their atmosphere. The composition of Pluto's haze is yet to be confirmed. The Venusian haze is not known, but it is likely to contain high concentrations of sulfur-containing molecules derived from SO_2 and H_2SO_4 (Takagi *et al.*, 2019). Therefore, Titan's atmospheric haze is the closest analogue to isoprene haze on habitable exoplanets; both are hydrocarbon-induced haze. To show that our results are not

specific to the case of Titan tholins, we compare our results with those using refractive indices of HCN (Khare *et al.*, 1994), C_2H_2 (Dalzell and Sarofim, 1969), and octane (Anderson, 2000).

We approximated the mean size distribution as a Gaussian distribution with a mean particle size equal adopted from the works of He *et al.* (2018) and Hörst *et al.* (2018), who measured the diameters of haze particles for different temperatures and metallicities. For CO_2-dominated and N_2-dominated atmospheres, we used a mean size of 89 nm and a standard deviation of 25 nm, which is approximated from the 300 K, 1000 × metallicity case from the work of He *et al.* (2018). For H_2-dominated atmospheres, we used a mean size of 53.8 nm and a standard deviation of 16 nm, which is approximated from the 300 K, 10,000 × metallicity case from the work of He *et al.* (2018). We choose to use a Gaussian distribution approximation rather than using the original measurement to avoid overfitting the data for isoprene.

Finally, we used miepython[**] to calculate the isoprene-induced haze's extinction cross-section with the assumed wavelength-dependent refractive indices and haze particle-size distribution. The cross-section is averaged from 1000 radii sampled from the Gaussian distribution. For simplicity, we assumed the haze particle to be spherical and we assumed the mean size and size distribution to be constant as a function of height.

3.2. Photochemistry model

We use the photochemical model from the work of Hu *et al.* (2012) to calculate the concentration of isoprene in exoplanet atmospheres as a function of surface production flux. The code includes photolysis, reactions with radicals and molecules, dry deposition to the surface, and rainout as sinks of atmospheric gases. The code has been validated by computing the atmospheric composition of current Earth and Mars, matching observations of major trace gases in both atmospheres. The photochemical model by Hu *et al.* (2012) has been used in a variety of papers (*e.g.*, Sousa-Silva *et al.*, 2020); we provide a brief summary description of our photochemical model here.

The Hu *et al.* (2012) photochemical model computes the steady-state chemical composition of a planetary atmosphere scenario. We have adapted the model to include isoprene, including photolysis, rainout, and reactions with $O^{\bullet}$, O_3, and $\bullet OH$ as sinks on isoprene. Due to the lack of reaction network studies for isoprene-induced radicals in anoxic environments, we assumed that fractions of the photochemical products of isoprene result in haze formation whereas the rest is not tracked; we note that this assumption formally underestimates isoprene concentrations, as haze will shield isoprene from UV photolysis. By contrast, our lack of a detailed reaction network means that we may omit chemical cycles by which the destruction of one molecule of isoprene may lead to additional destruction; this may lead to overestimates of isoprene concentrations. More detailed characterization of the reactions of isoprene and its products are required to resolve this challenge. In Section 4.3, we discuss how different assumed haze-to-isoprene mass fractions (from 1 ppm to 10%) will impact the effect of haze on the transmission spectra. We assume the mass fraction to be constant as a function of height.

The model handles more than 800 chemical reactions (and photochemical reactions), formation, and deposition for aerosols (including elemental sulfur and sulfuric acid); our exoplanet scenarios (Section 3.3) employ a subset of ~450 of the reactions, excluding primarily nitrogen chemistry and high-temperature reactions (see Hu *et al.*, 2012 for the rationale for these choices). The model also treats dry and wet deposition, thermal escape, and surface emission. The model is flexible to simulate both oxidized and reduced conditions. The model uses delta-Eddington two-stream method to compute the UV and visible radiation in the atmosphere. The optical depth used is calculated with molecular absorption, Rayleigh scattering, and aerosol Mie scattering.

The stellar UV spectral flux data is an input for the photochemistry code. We take the input stellar fluxes from the work of Seager *et al.* (2013). For the UV flux from a solar-type star, Seager *et al.* (2013) used the Air Mass Zero (AM0) reference spectrum produced by the American Society for Testing and Materials (http://rredc.nrel.gov/solar/spectra/am0) with the average quiet-Sun emission spectrum from the work of Curdt *et al.* (2004), in total covering the wavelength range from 110 nm to 10 μm. For the M dwarf star, we used the measured spectrum for GJ 1214 b from 115 to 300 nm (France *et al.*, 2013), and the 3000 K NextGen model spectrum at >300 nm (Allard *et al.*, 1997).

3.3. Simulation scenarios

We now describe our exoplanet benchmark scenarios. Our exoplanet benchmark scenarios are based on those in the works of Hu *et al.* (2012) and Seager *et al.* (2013); they are also used in the work of Sousa-Silva *et al.* (2020). Later, we discuss in detail the 6 simulation scenarios considered here, representing H_2-dominated, N_2-dominated, and CO_2-dominated atmosphere, each exposed to a Sun-like star and an M dwarf star.

3.3.1. Astronomical scenarios.

We consider stellar irradiation environments corresponding to the modern Sun and an M5V star (''M dwarf star'') with a visual magnitude of 10.

The semimajor axes of the planets are taken to be 1.6, 1.0, and 1.3 AU if orbiting a Sun-like star, and 0.042, 0.026, and 0.034 AU if orbiting an M dwarf star for H_2-dominated, N_2-dominated, and CO_2-dominated atmosphere, respectively. The semimajor axes are chosen to maintain a surface temperature of 288 K (Hu *et al.*, 2012).

We calculate photochemical models for an Earth analog planet (1 Earth-mass, 1 Earth-radius). We follow the work of Hu *et al.* (2012) in projecting these photochemical models to the scenario of a massive super-Earth with 10 Earth-mass and 1.75 Earth-radius, by assuming the molecular mixing ratio to be a function of pressure, which is invariant of surface gravity. The preference for the larger planet is beneficial for observation with near-future space

[**]Miepython (https://github.com/scottprahl/miepython) is a python implementation of fast extinction cross-section calculation described in Wiscombe (1979). We note that the imagery part of the refractive index is taken as a negative number in miepython.

telescopes for mass measurement with radial velocity and atmosphere characterization with both transmission (*e.g.*, more likely to retain a reducing, H_2-dominated atmosphere) and secondary eclipse spectroscopy (*e.g.*, higher planet/star flux ratio).

3.3.2. Atmospheric scenarios. We consider three different atmosphere scenarios according to their redox state: a reducing H_2-dominated atmosphere, an intermediate redox state N_2-dominated atmosphere, and a weakly oxidizing CO_2-dominated atmosphere. We only consider anoxic atmospheres, because it is already well known from the Earth's atmosphere that isoprene cannot accumulate in an O_2-dominated atmosphere. The exact composition and vertical mixing ratio profile for the starting atmosphere scenarios that we use as seeding conditions for calculating vertical mixing ratio profiles with varying surface flux are shown in Supplementary Appendix A1 (and originally come from Sousa-Silva *et al.*, 2020) for details on the H_2-dominated and CO_2-dominated atmosphere scenarios. The physical concept behind the H_2-dominated atmosphere scenario is that the planet outgassed H_2 during planet formation and managed to either maintain its H_2 atmosphere or has interior reservoirs with planetary processes to replenish it (Table 1).

3.3.3. Atmosphere temperature, pressure, and abundances. Using the six starting simulation scenarios (three atmosphere scenarios for the Sun-like star and three for the M dwarf star) as seeds, we calculate the mixing ratio profile of isoprene with varying surface flux by using the photochemistry code from the work of Hu *et al.* (2012) for each scenario. The vertical mixing strength (Eddy diffusion profile) of an atmosphere archetype is linearly scaled from the ratio of the Earth atmosphere's mean molecular mass and the atmosphere archetype. We adopt the eddy diffusion coefficients scaling factors of 6.3, 1.0, and 0.68 for the H_2-, N_2-, and CO_2-dominated atmospheres from the work of Hu *et al.* (2012), which is based on the scale height of the atmosphere archetypes.

Table 1. Atmosphere Composition Adopted from Photochemistry Output of Hu *et al.* Model for the Six Simulation Scenarios Considered

Atmosphere archetypes	*Stellar type*	*Main composition*
H_2-dominated	Ma	H, **H_2**, O, CH_4, **H_2O**, **N_2**, **CO**, O_2, **CO_2**
	Sun	H, **H_2**, O, CH_4, **H_2O, N_2**, **CO**, O_2, **CO_2**, C, CH_3, C_2H_2, C_2H_6,
N_2-dominated	Ma	H, **H_2**, **O**, CH_4, **H_2O, N_2, CO**, O_2, **CO_2**
	Sun	H, **H_2**, **O**, CH_4, **H_2O, N_2**, CO, O_2, **CO_2**, C
CO_2-dominated	Ma	H, **H_2**, **O**, CH_4, **H_2O, N_2, CO, O_2, CO_2**, H_2O_2, O_3
	Sun	H, **H_2, O**, CH_4, **H_2O, N_2**, **CO**, **O_2, CO_2,**

For spectroscopy calculation and detection assessment, we only consider molecules that have reached a local mixing ratio of at least 100 ppb at any height in the atmosphere. Molecules that fail to meet this mixing ratio criterion are unlikely to contribute sufficient opacity to the simulated transmission and emission spectra and are, therefore, not included. Molecules more than 100 ppm at any height are marked in bold. For detailed mixing ratio profile, see Supplementary Appendix Fig. A1. Addition of isoprene may drastically change the mixing ratio profile for some molecules (see Fig. 9).

C_2H_6 = ethane; CH_4 = methane.

Adapted from Hu *et al.* (2012).

The surface pressure of the planet is set to 1 bar, and the surface temperature is set to 300 K. In the troposphere, the temperature decreases with altitude based on a dry adiabatic lapse rate. The tropopause is set to 160 K for the H_2-dominated atmospheres, 180 K for the CO_2-dominated atmospheres, and 200 K for the N_2-dominated atmospheres. The different tropopause temperatures used for each atmosphere reflect the different efficiencies of gases as coolants in the upper atmosphere. H_2 is a more effective coolant than N_2, so the stratosphere of H_2-dominated atmospheres will be colder than N_2-dominated atmospheres.

Temperatures above the troposphere are set to be constant, that is, no temperature inversion (see Supplementary Appendix A1 for the temperature-pressure profiles for the three-atmosphere archetypes). This assumption may be violated for hazy atmospheres, where absorption of UV photons by high-altitude haze may drive an inversion, analogous to ozone in the modern Earth's atmosphere. We expect our results to be relatively insensitive to the stratospheric temperature since the ultimate limit on accumulation of isoprene comes from UV photolysis. Nevertheless, we performed a sensitivity test of the resulting transmission spectra by replacing the temperature-pressure profile with that of the Earth's temperature-pressure profile. We find that there is negligible difference in the transmission spectra resulting from the two different temperature-pressure profiles.

We exclude trace gases that do not exceed 100 ppb at any altitude from our spectral model, because their absorption does not contribute enough variation to the atmosphere spectra and they are unlikely to be detectable without significant instrumentation advancements that are capable of reaching $a < 1$ ppm noise floor.

3.4. Atmosphere spectra simulation

To assess the detection of trace gases and biosignature gases in exoplanet atmosphere scenarios, we constructed the ''Simulated Exoplanet Atmosphere Spectra'' (SEAS; https://github.com/zhuchangzhan/SEAS) model to simulate transmission and secondary eclipse thermal emission spectroscopy following the principles described in the work of Seager *et al.* (2013). The methods for calculating spectra are similar to those described in in the works of Miller-Ricci *et al.* (2009) and Kempton *et al.* (2017). SEAS accepts user-input temperature-pressure profiles and mixing ratio profiles; the mixing ratio profiles are especially important for the study of super-Earth atmospheres, as they are severely impacted by photochemistry and atmosphere chemistry.

The molecular cross-sections used by SEAS are interpolated from a pre-generated grid of cross-sections for a grid of pressure (10^5 to 10^{-2} Pa in multiples of 10) and temperature (150–400 K in steps of 25 K). For molecules that have line lists from the work of Gordon *et al.* (2017), the cross-sections are calculated by using the HAPI package

(Kochanov *et al.*, 2016). For molecules that have line lists in ExoMol (Tennyson *et al.*, 2016; Gordon *et al.*, 2017), cross-sections are calculated by using the ExoCross package (Yurchenko *et al.*, 2018).

We validated SEAS by generating Earth spectra and comparing transmission spectra results with data from the Atmospheric Chemistry Experiment data set (Bernath *et al.*, 2005) and comparing emission spectra with results from MODerate resolution atmospheric TRANsmission spectrum simulation code (Berk *et al.*, 1998).

3.4.1. Transmission spectra. The SEAS transmission spectrum code calculates the radiative transfer of stellar radiation passing through each layer of the transiting planet atmosphere. Next, we detailed the exact step to calculate the effective height of the atmosphere and the transit depth for each wavelength.

(1) We defined each layer of the atmosphere with a height of 1 scale height starting from the surface to the top of the atmosphere and assumed local thermodynamic equilibrium within each layer of the atmosphere.
(2) Since the atmosphere is taken to be homogenous within each layer, we approximate the three-dimensional spherical shell as a two-dimensional ring.
(3) Since each layer is curved and stellar radiation is radial, the stellar radiation along the limb path of each layer will penetrate sections of the current layer and sections of layers above the current layer. Therefore, the optical depth of each layer is the sum of the optical depth through each section as follows:

$$A(\lambda)_i = \sum_{i}^{z} \sum_{j=0}^{m} n_{i,j}(P,\ T) \cdot \sigma_{i,j}(P,\ T,\ \lambda) \cdot l_i \qquad (4)$$

where $A(\lambda)_i$ is the total wavelength-dependent absorption for the i th layer, j denotes each molecule, n is the number density, $\sigma(\lambda)$ is the wavelength-dependent absorption cross-section, P is the pressure, T is the temperature, l is the path length, z denotes the total number of layers above the i th layer that the stellar radiation passes through, and m denotes the total number of molecules.

(4) The transmission by each layer is calculated by using Beer-Lambert's Law: $T = e^{-A}$, and absorbance is $1\text{-}T$.
(5) The effective height of the atmosphere is calculated by summing the effective height of each layer, which is calculated by multiplying the absorbance by the scale height of each layer.
(6) The transit depth of the atmosphere is calculated by summing the flux attenuated by each layer of the atmosphere, which is calculated by multiplying the absorbance by the cross-sectional area of each layer.

We note that the cross-sections of haze particles have units of (cm^2/particle) and, therefore, the particle density is calculated from the gas number density and has a unit of (particle/cm^3). The particle density of isoprene-induced haze at a given layer is calculated by dividing the particle vapor density with the average particle mass. The particle vapor density is the product of the air density, the mixing ratio of isoprene, and an assumed haze-to-isoprene mass fraction (see Section 3.2).

To consider the detection of isoprene via transmission spectra, we first assessed model scenarios in which the atmospheres have no clouds or haze. This result represents an upper bound on the detectability of the isoprene features in transmission (Section 4.2). Next, we study how detection will be hindered if haze is included (Section 4.3).

3.4.2. Secondary eclipse thermal emission spectroscopy. The SEAS thermal emission code is similar to those described in the works of Seager (2010) and Sousa-Silva *et al.* (2020) and uses the same temperature-pressure profiles, mixing ratio profiles, and molecular-cross sections as in the transmission code.

The emission code integrates the blackbody radiation for each wavelength from the surface and up through each layer of the atmosphere, as the radiation is absorbed and reemitted by gases in each layer. The surface is set to be a pure black body, and the top layer is set to be transparent. We do not consider scattering in the current emission code. The final spectrum is calculated by integrating the emerging flux by the cross-sectional area of the planet. To add the presence of clouds, we consider 50% cloud coverage by averaging between a cloudy and cloud-free spectrum.

3.5. Simulated exoplanet observation

We simulate observations of the six simulation scenarios as described in Section 3.3.2 with varying amounts of isoprene as computed by our photochemistry model in Section 3.2. We used the astronomical parameters defined in Section 3.3.1 and a 10 M_{Earth}, 1.75 R_{Earth}-planet transiting a star with a K-band apparent magnitude of 10 (JWST observes in near-mid IR). The star can be either (1) a Sun-like star or (2) a 3000 K, 0.26-R_{sun} M dwarf star.

Since isoprene has many broad spectral features spanning a wide range of wavelength as discussed in Section 3.1.2, we opt to assess the detection of isoprene by using JWST's Near InfraRed Spectrograph (G140M, G235M, G395M) and MIRI (LRS) observation modes.

For transmission spectroscopy, we combined the simulated spectra from SEAS and observational noise simulated by using Pandexo (Batalha *et al.*, 2017), the community JWST exposure time calculator, and noise simulator. To account for potential unknowns, we added a 10 ppm noise floor as suggested by Batalha *et al.* (2017).

For secondary eclipse thermal emission spectroscopy, we approximate our telescope specifications based on JWST and the use of the NIRSpec and MIRI instruments (Bagnasco *et al.*, 2007; Wright *et al.*, 2010), or a 6.5 m space telescope with a quantum efficiency of 25%. Since stellar flux is the source of the noise, we do not model instrumental noise and instead used a 50% photon noise multiplier. Finally, we compute the signal-to-noise ratio for each bin by using the equation given next:

$$\boldsymbol{SNR} = \frac{|\boldsymbol{F_{out}} - \boldsymbol{F_{in}}|}{\sqrt{\boldsymbol{\sigma}^2_{\boldsymbol{F_{out}}} + \boldsymbol{\sigma}^2_{\boldsymbol{F_{in}}}}} \qquad (5)$$

where F_{in} is the flux density within the absorption feature, F_{out} is the flux density of the surrounding continuum of the feature, and σF_{out} and σF_{in} comprise the respective uncertainty.

Although we have estimated instrumental noise, our estimates on stellar noise remain rudimentary. We raise the caveat that additional sources of astrophysical noise may make detecting molecular features challenging. Other astrophysical phenomenon, such as non-homogeneity of stellar disks, could introduce false spectral features from 0.3 to 5.5 μm with intensities around 70 ppm for M5V stars (Rackham *et al.*, 2018), potentially hindering the detection of biosignature gases.

3.6. Biosignature gas detectability assessment

Determining the detectability of a biosignature gas in our atmosphere scenarios is expanded based on the methods defined in the works of Seager *et al.* (2013), Tessenyi *et al.* (2013), and Sousa-Silva *et al.* (2020), where we assess whether the spectral features of the target biosignature gas can be identified within a reasonable number of transit (secondary eclipse) observations.

First, we assess whether or not the atmosphere (and the biosignature gas) can be detected by applying a null-hypothesis test. More specifically, we assess whether or not the simulated wavelength-dependent transit depth data can be explained with a straight line (transmission) or with a blackbody radiation curve (emission). If so, then the simulated observation cannot pass the null-hypothesis test and we deem the atmosphere scenario to be not-detectable.

Next, if the simulated observation for the atmosphere scenario passed the null hypothesis, we then compare the goodness-of-fit of a model atmosphere that contains the biosignature gas and a model atmosphere without the biosignature gas. The goodness-of-fit is computed by using the reduced chi-square statistic using the following equation:

$$\chi_v^2 = \frac{\chi^2}{v} = \frac{1}{v} \cdot \left[\sum_i \frac{(O_i - C_i)^2}{\sigma_i^2} \right] \tag{6}$$

where χ_v^2 is the reduced chi square, v is the degree of freedom (or the number of wavelength bins), χ^2 is the chi squared, O_i is the simulated observational data, C_i is the simulated model, σ_i is the variance (or error as calculated from Pandexo noise simulator for a specific instrument), and finally i denotes each wavelength bin. We note that binning the spectra reduces the variance at the expense of reducing the degree of freedom.

The simulated observation data has moderate spectral resolution ($R > 1000$ for NIRSpec and $R = 160$ for MIRI) but also has large error bars for each data point. Since we are interested in detecting the broad spectral features of isoprene and not the narrow, detailed individual features, we can trade resolution for increased *SNR* to improve our model's goodness-of-fit. $R = 10$–20 is where isoprene becomes indistinguishable with methane for features at shorter wavelengths (<4 μm), and this concept will be further explored in Section 4.3.

Finally, we repeat calculation of the detection metric cited earlier by binning down our simulated spectra to spectral resolutions of $R = 10$, 20, 50, and 100 to find the most optimal choice and iterate from 1 to 100 transits until detection is reached. If no detection is found with any spectral resolution and 100 transits (theoretical upper limit for a planet in the habitable zone of an M dwarf star given JWST's expected cryogenic lifetime of 5 years), we deem the spectral features not detectable.

4. Results

Despite its promising potential, isoprene does not satisfy all criteria to be a good biosignature gas. Namely, isoprene is unable to accumulate in the upper atmosphere at even 10 times the Earth's production level, and in fact isoprene must enter a ''run-away phase'' to accumulate to detectable abundances. In addition, isoprene can be spectrally indistinguishable from methane at short wavelengths (<4 μm) with JWST's spectral resolution. Regardless of this, isoprene should still be added into the roster of biosignature gas to be considered in future studies because isoprene has no abiotic false-positives and it has the potential to be produced in large quantities as it is by life on the Earth.

We demonstrate that with the Earth's production rate, isoprene molecules are predominantly concentrated near the surface (<10 km) (Section 4.1.1), making detection impossible with near-future technologies (Section 4.2.1). An additional key point is that with a production rate 100–1000 times higher than the Earth's isoprene production rate—which we assert is challenging but within reasonable estimates (Section 4.1.2)—isoprene can enter a run-away phase, enabling isoprene molecules to populate the upper atmosphere at a significant concentration (>100 ppm) (Section 4.1.3) and become detectable (Section 4.2.2).

Unfortunately (within the context of observing the atmosphere of a super-Earth with JWST), despite its detectability in a run-away phase, we show that isoprene's spectral features can be confused with those of methane and other hydrocarbons More specifically, isoprene spectral features at 3.1–3.7 μm overlap with that of methane. Moreover, isoprene's spectral features at 9–12 μm lie in a wavelength region populated by hundreds of other hydrocarbon gases (Section 5.2). On the Earth, any isoprene is immediately converted into haze, so we also discuss the impact of haze on hindering the detection of isoprene (Section 4.3).

Far-future telescopes that can achieve detection at higher spectral resolution than JWST may make detection of isoprene possible. Therefore, given the abundant chemical reactions involving isoprene in known biochemistry and the fact that it does not have any abiotic false positives (Section 4.3), it would be hasty to discard isoprene as a potential biosignature gas.

4.1. Isoprene accumulation

We calculated the column-averaged mixing ratio profile of isoprene and other gases as a function of surface isoprene flux, using the photochemistry code described in Section 3.3. We list the column-averaged mixing ratio for isoprene given the surface production rate for each simulation scenario in Table 2.

To assess isoprene's ability to accumulate in an atmosphere, we first examine the distribution of isoprene in an exoplanet atmosphere given a production rate similar to that on the Earth, $\sim 3 \times 10^{10}$ molecules/(cm^2·s) (Section 4.1.1). Next, to go beyond the Earth's conditions, we calculate isoprene mixing ratio profile for a range of isoprene surface production rates. We vary the production rate from 10^3

Table 2. Isoprene Column-Averaged Mixing Ratios (in Units of ppm) Corresponding to Various Isoprene Surface Fluxes (*i.e.*, Production Rates) for Our Six Atmosphere Archetypes

Atmospheric scenario	*H_2-dominated*		*N_2-dominated*		*CO_2-dominated*	
P_{iso} /stellar type	*M dwarf*	*Sun like*	*M dwarf*	*Sun like*	*M dwarf*	*Sun like*
10^{10}	0.0006	/	0.0002	/	0.0016	/
10^{11}	0.050	/	0.0079	/	6.22	/
10^{12}	3.30	/	1.98	/	635.81	/
10^{13}	865.41	0.001	4426.8	0.0001	7341.80	0.075
10^{14}	/	0.040	/	/	/	1.84
10^{15}	/	24.95	/	/	/	46.78

For reference, biological production of isoprene on Earth is $\sim$500 Tg/year, or 2.7×10^{10} molecules/(cm$^2\cdot$s) and biological production of CH_4 on Earth is also about 500 Tg/year, or 1.2×10^{11} molecules/(cm$^2\cdot$s). Our photochemistry model simulated equilibrium atmospheric abundances for a range of surface fluxes from 10^3 to 10^{15} molecules/(cm$^2\cdot$s). Fluxes $<10^{10}$ and $<10^{13}$ molecules/(cm$^2\cdot$s) are omitted for M dwarf star and Sun-like stars, respectively, because the resulting column-averaged mixing ratios are negligible (<1 ppb). Fluxes $>10^{13}$ molecules/(cm$^2\cdot$s) are omitted for M dwarf stars, because isoprene reaches a run-away phase and to exceed 1% of the atmosphere by volume, a likely unrealistic value. Omitted entries are denoted by the "/" symbol. The column-averaged mixing ratio quickly transitions from <1 to >100 ppm around 10^{12}–10^{13} molecules/(cm$^2\cdot$s) surface flux values.

molecules/(cm$^2\cdot$s) to 10^{15} molecules/(cm$^2\cdot$s) in steps of 10. We choose a maximum of 10^{15} molecules/(cm$^2\cdot$s) to represent the highest isoprene production rate found in a niche environment on Earth (Section 4.1.2).

4.1.1. Isoprene remains a trace gas at Earth's production rate. At the Earth's isoprene production rate of 3×10^{10} molecules/(cm$^2\cdot$s), isoprene remains a trace gas in all of the three exoplanet atmosphere scenarios, at <1 ppb (column-averaged mixing ratio) (Table 2). At surface fluxes lower than 1×10^{11} molecules/(cm$^2\cdot$s), isoprene is concentrated near the surface where it is created. Any isoprene that diffuses to the upper atmosphere is readily destroyed. To illustrate this finding, the column-averaged mixing ratio of isoprene at four different altitudes for a CO_2-dominated atmosphere of an exoplanet transiting an M dwarf star is shown in Fig. 9.

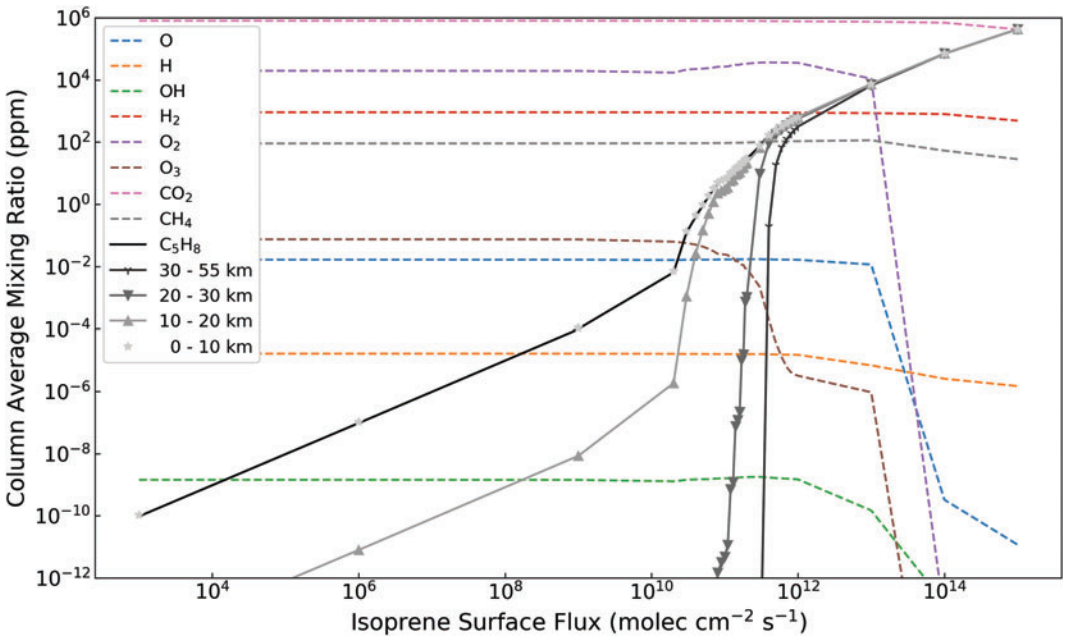

FIG. 9. Column-averaged mixing ratios of isoprene and other major atmospheric gases in a CO_2-dominant atmosphere orbiting an M dwarf star as a function of isoprene surface flux. Dominant atmosphere species and isoprene-reacting radicals are plotted in various colored dash lines. The isoprene column-averaged mixing ratios (in units of ppm) for different isoprene surface fluxes [*i.e.*, biological production rate; in units of molecules/(cm$^2\cdot$s)] are shown by a solid black curve. The abundance of isoprene at 0–10 km from the surface overlap with the solid black curve and is additionally indicated by the light gray stars. The abundances of isoprene at 10–20, 20–30, and >30 km from the surface are shown in different shades of gray and are additionally shown by different types of triangles. For low surface fluxes, isoprene remains a trace gas throughout the atmosphere (<ppm levels) with abundances increasing linearly with surface fluxes. For surface fluxes above 3×10^{10} molecules/(cm$^2\cdot$s), isoprene abundance rapidly increases. For isoprene surface fluxes above 3×10^{11} molecules/(cm$^2\cdot$s), isoprene abundance at the upper atmosphere (where most transmission spectral features originate) reaches the same level as surface abundance. Color images are available online.

Isoprene may remain a trace gas even at higher production rates than on the Earth, because large isoprene sinks may exist on planets different from the Earth. The sinks could realistically include life that has evolved to consume the abundant isoprene; photochemical destruction pathways as yet-unknown in anoxic atmospheres; and/or higher deposition rates than those that exist on the Earth.

As a trace gas, isoprene is not detectable via transmission spectroscopy even with far-future space telescopes. In Section 4.2.1, we explore the potential to detect isoprene as a trace gas via thermal emission spectroscopy by using JWST.

4.1.2. Maximum isoprene production estimate. For isoprene to accumulate to higher levels than a trace gas, it must be produced by life at rates hundreds, if not thousand times, the global production rate on the Earth (Fig. 9). In this section we establish that high isoprene production niche environments exist on the Earth, up to one million times the Earth's globally averaged isoprene production rate (Section 2.2).

One such niche is a modern tropical environment, where isoprene production is optimal for trees, the main producer of isoprene on the Earth due to their widespread abundance. In the Amazon rainforest, African rainforest, and Southeast Asia, the isoprene production rate averages $>1\,\mathrm{mg/(m^2\cdot s)}$ with core areas averaging $>10\,\mathrm{mg/(m^2\cdot s)}$ (McFiggans *et al.*, 2019). In comparison, the global averaged isoprene production rate on the Earth is $\sim 3\times10^{-5}$ $\mathrm{mg/(m^2\cdot s)}$ [converted from 500 Tg/year, or $\sim 3\times10^{10}$ $\mathrm{molecules/(cm^2\cdot s)}$]. For 12% of the Earth's habitable history [*e.g.*, during Phanerozoic eon (the past 541 million years)], the Earth had a pole-to-pole tropical climate (*e.g.*, during Carnian Pluvial Event; Royer *et al.*, 2004; Dal Corso *et al.*, 2012). Therefore, in a hypothetical scenario where the Earth's total land mass ($\sim$30% of total surface area) is filled completely with isoprene producers and attains the $1\,\mathrm{mg/m^2}$ production rate, it is possible for the global average to reach $0.3\,\mathrm{mg/(m^2\cdot s)}$, or 3×10^{14} $\mathrm{molecules/(cm^2\cdot s)}$. However, although trees are the main producer of isoprene on the Earth, we cannot ignore the fact that trees are also the main producer of oxygen and the presumed condition for isoprene to accumulate is an anoxic atmosphere.

For a purely anoxic environment, we assume an Archean biosphere that comprises anaerobic, isoprene-producing prokaryotes such as those found in lab studies (Fall *et al.*, 1998) (see Section 2.2 for details), which is capable of naturally producing isoprene in high quantities with average production rates of $50\,\mathrm{nmol/(g\cdot hour)}$. By using an average bacteria density of $1\,\mathrm{g/cm^3}$ (Loferer-Krößbacher *et al.*, 1998) and assuming a global biomass layer of 1 cm thick covering all of the Earth's total land mass ($\sim$30% total surface area), it is possible for the global average to reach 2.5×10^{13} $\mathrm{molecules/(cm^2\cdot s)}$.

With these assumptions, we show that the high isoprene production rates required for isoprene to accumulate in the upper atmosphere can be supported by species on Earth and the theoretical upper limit to isoprene production rate is 10^4 that of the Earth's current production rate. Therefore, it is plausible to explore the detection of isoprene under these conditions.

4.1.3. Isoprene run-away. Very high surface fluxes of isoprene will send isoprene accumulation into a run-away state (Fig. 9). In a run-away phase, isoprene rapidly accumulates in the upper atmosphere to high levels, up to hundreds of ppm. The run-away is a result of ''photochemical self-shielding'' whereby the isoprene production flux saturates its UV-driven sinks, resulting in a dramatic increase in lifetime and hence accumulation. This run-away phenomena has been discussed for abiotic CO (Kasting *et al.*, 1983, 1984, 2014; Zahnle, 1986; Kasting, 2014), has been alluded to for CH_4 (Segura *et al.*, 2005), and has been observed by us for other biosignature gases (Huang *et al.*, unpublished data; Sousa-Silva *et al.*, 2020). We plan a detailed study in the work of Ranjan *et al.* (unpublished data). In this subsection, we consider the case where isoprene has entered a run-away phase, a scenario in which the abundance of isoprene in the upper atmosphere reaches a similar level to the abundance of isoprene in the lower atmosphere.

The run-away phase is important, because it shows that cases exist in which isoprene can populate the upper exoplanet atmosphere such that it can be detected via transmission spectroscopy in simulations of the JWST. Recall that transmission spectra are only sensitive to the upper atmosphere. The lower atmosphere has extremely long path lengths for light to travel through it, making the atmosphere optically thick, which, in turn, results in featureless spectra.

The most favorable atmosphere scenario for isoprene accumulation is a CO_2-dominated atmosphere because CO_2 shields isoprene more strongly from UV irradiation than N_2-dominated atmosphere or H_2-dominated atmosphere do.

The run-away effect is highly dependent on the quantity of UV flux from the host star. UV fluxes from Sun-like stars are significantly (more than 1000 times) higher than UV fluxes from M dwarf stars. Isoprene is unlikely to enter the run-away phase for planets orbiting Sun-like stars. There, the production rate required is around 3×10^{14} $\mathrm{molecules/(cm^2\cdot s)}$ for a CO_2-dominated atmosphere, approaching the maximum isoprene production rate even in niche environments on the Earth. In contrast, for planets orbiting M dwarf stars, isoprene's transition to the run-away phase occurs around 3×10^{11} $\mathrm{molecules/(cm^2\cdot s)}$ for a CO_2-dominated atmosphere and 1×10^{12} $\mathrm{molecules/(cm^2\cdot s)}$ for an H_2-dominated or N_2-dominated atmosphere. The surface flux required to enter the run-away phase is within 1–2 orders of magnitude of the Earth's globally averaged surface isoprene flux of 2.7×10^{10} $\mathrm{molecules/(cm^2\cdot s)}$. With isoprene surface fluxes above 3×10^{11} $\mathrm{molecules/(cm^2\cdot s)}$, but below 3×10^{12} $\mathrm{molecules/(cm\cdot s)}$, the corresponding atmosphere volume mixing ratio is 100 ppm or greater, and isoprene can accumulate in the upper atmosphere. At isoprene surface fluxes above 3×10^{12} $\mathrm{molecules/(cm^2\cdot s)}$, the corresponding atmosphere column-averaged volume mixing ratio is 1000 ppm (0.1%) or greater. There are sufficient isoprene molecules in the atmosphere to balance photochemical destruction, thus allowing isoprene molecules to diffuse to the upper atmosphere; the resulting mixing ratio profile is well mixed such that isoprene has a constant mixing ratio up to 50 km above the surface.

Therefore, if life produces enough isoprene to enter a run-away phase, isoprene can accumulate to become a major atmospheric gas. In this case, life will have re-engineered the atmosphere, reminiscent of cyanobacteria's oxygenation

of the Earth's atmosphere. We note that the run-away hypothesis ignores potential unknown chemical or surface sinks in anoxic atmospheres that would limit the accumulation of isoprene in the atmosphere. Therefore, realistic situations might require further investigation (see *e.g.*, Ranjan *et al.*, unpublished data).

4.2. Isoprene detectability in exoplanet atmospheres

Isoprene detectability can be separated into two categories. The first category is where isoprene does not enter a run-away phase and remains a trace gas (*i.e.*, does not accumulate above a column-averaged mixing ratio of 1 ppm). The second category is where isoprene is a major atmospheric gas, resulting from its production by life at high enough levels that isoprene enters a run-away phase (*i.e.*, isoprene accumulates above a column-averaged mixing ratio of 100 ppm). The transition from a column-averaged mixing ratio of 1–100 ppm occurs rapidly as a function of surface flux (Fig. 9), so we omit discussion of this transition phase.

4.2.1. Detecting isoprene as a trace gas is challenging. As a trace gas, isoprene molecules are concentrated near the surface. We did not find any transmission spectra scenario in which isoprene can accumulate above the troposphere for a surface flux below 1×10^{12} molecules/(cm$^2\cdot$s). Our spectra simulations confirmed that the isoprene spectral features are <10 ppm in transit depth, smaller than JWST's assumed noise floor. Therefore, it is not possible to detect isoprene as a trace gas via transmission spectroscopy.

We additionally explore whether isoprene can be detected via secondary eclipse thermal emission spectroscopy (emission spectroscopy) for planets transiting an M dwarf star. In emission spectroscopy, spectral features scale with the temperature gradient and, in general, detection might be more promising than for transmission spectroscopy.

For the terrestrial exoplanet atmosphere scenarios we considered in this study, the largest change in temperature occurs in the lower atmosphere layers, from the planet surface to ''tropopause.'' Therefore, in scenarios where isoprene is a trace gas and concentrated near the surface, it is worth investigating detection via emission spectroscopy.

Since isoprene accumulates best in CO_2-dominated atmospheres, we modeled this case. We found that in a CO_2-dominated atmosphere, secondary eclipse detection for a planet transiting an M dwarf star is possible given a surface flux of 1×10^{11} molecules/(cm$^2\cdot$s), which is three times that of the Earth's isoprene surface flux (Fig. 10). Detection of isoprene in H_2- and N_2-dominated atmospheres is possible given a surface flux of 1×10^{12} molecules/(cm$^2\cdot$s). For a planet with a habitable surface temperature of $\sim$300 K, the peak thermal emission is between 10 and 15 μm. There is only one very broad spectral feature of isoprene that lies in this spectral region, between 9 and 12 μm.

Unfortunately, given a spectral resolution of R, approximately 10–20, although we could detect isoprene, it would be hard to distinguish isoprene from other molecules that could be absorbing in this spectral region. Future 30-meter diameter aperture ground-based telescopes with dedicated instruments that focus on the N-band and using a spectral resolution of $R>100$ will be able to identify the individual, narrow spectral features that made up the broad 9–12 μm spectral features if given generous observation time (100+ transits).

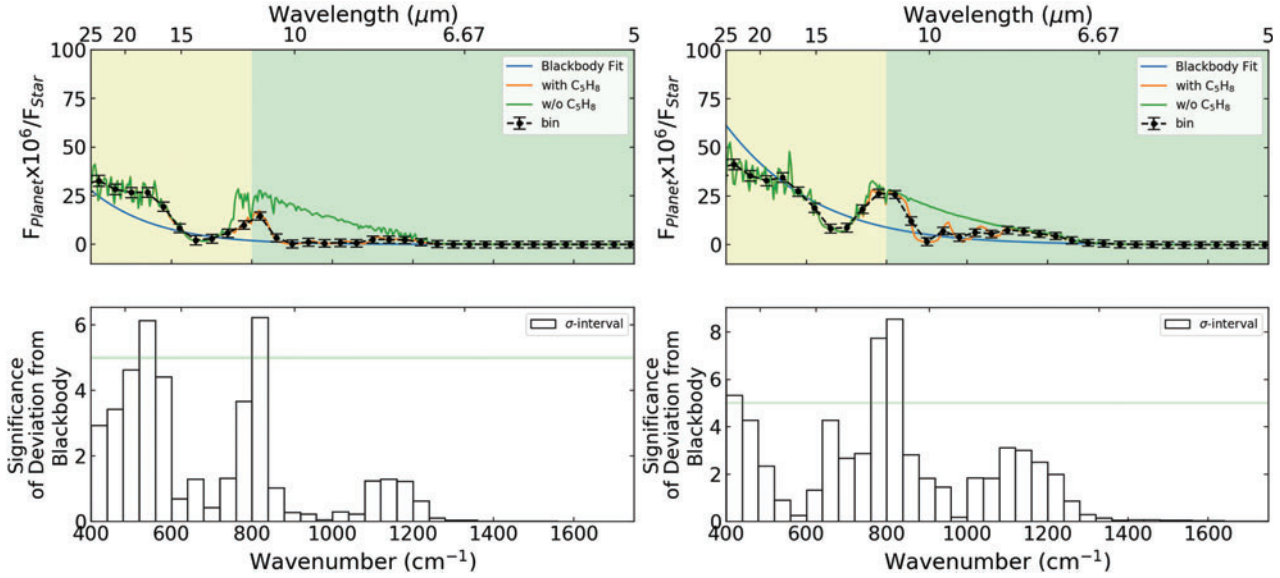

FIG. 10. Simulated secondary eclipse thermal emission spectra for an H_2-dominated (left) and N_2-dominated (right) atmosphere of an exoplanet transiting an M dwarf star with an isoprene surface flux of 1×10^{12} molecules/(cm$^2\cdot$s). The simulated atmosphere uses input and parameters as listed in Section 3. We show the planet-to-star flux ratio versus wavelength in μm (top) and the statistical significance of a modeled atmosphere versus wavenumber in cm^{-1} (bottom). The horizontal axes are applied to both the top and bottom panel. In the top panel, we show the simulated atmospheres with and without isoprene as represented by the green and orange curves, respectively. The best fit blackbody curves are shown in blue. Simulated observations of atmospheres with isoprene are represented by the black error bars. In the bottom panel, we show the statistical significance of a simulated atmosphere with isoprene as compared with the black body fit, in units of σ-interval. The green line represents the 5-σ statistical significance threshold. Color images are available online.

4.2.2. Detection of isoprene as a major atmospheric gas. We assess the detection of isoprene via transmission spectra for isoprene in the run-away phase via transmission spectra. For exoplanets with anoxic atmospheres orbiting M dwarf stars, the high isoprene accumulation scenario occurs given an isoprene production rate of at least 1×10^{12} molecules/(cm$^2\cdot$s) for any atmosphere scenario we studied. We found that at this high production rate, isoprene can accumulate to a column average mixing ratio of 100–1000 ppm and the isoprene spectral features would be prominent compared with those of other molecules, potentially allowing isoprene to be identified (Fig. 11).

For terrestrial exoplanets transiting the 10th magnitude M5V dwarf star, only the H_2-dominated atmospheres (with surface pressure set to 1 bar and surface temperature set to 300 K) are detectable with JWST in transmission spectroscopy in near- to mid-IR, as they have a large scale height due to the low mean molecular weight. In this scenario, isoprene can be detected if it is produced at fluxes above 3×10^{12} molecules/(cm$^2\cdot$s), or 100 times that of the Earth's isoprene production rate. Isoprene has many spectral features; we find that detection can be achieved with 20 transits by using any of the four modes of JWST (NIRSpec G140M, G235M, G 395M, and MIRI LRS) we assessed (Fig. 12).

For N_2-dominated and CO_2-dominated atmospheres, we did not find a scenario in which the atmosphere is detectable via transmission spectroscopy with JWST without investing 100 transits per observation mode. Although it is theoretically possible to accumulate 100 transits for a planet orbiting a late M dwarf star over 5 years (the cryogenic lifetime of JWST), it is unrealistic given the competitive nature of the telescope observation time. We, therefore, conclude that detection of isoprene in a non-H_2-rich atmosphere should only be considered plausible for exoplanet dedicated future observatories with far better collecting power.

For exoplanets transiting a Sun-like star, we found that no atmosphere scenarios are detectable via transmission spectroscopy because the ratio of planet to star radius, or $(R_{planet}/R_{star})^2$, was too small, resulting in too small a transit depth even for H_2-dominated atmospheres.

Assessing the detectability of isoprene as a major atmospheric gas via secondary eclipse thermal emission spectroscopy is at present problematic due to our assumption of an isothermal atmosphere above the 0.01 bar (10^3 Pa) level (an assumption in our photochemistry model; Hu *et al.*, 2012). Secondary eclipse thermal emission spectra can, in principle, arise in the lower atmosphere, which in our model does have a temperature gradient. However, when isoprene is a major atmosphere gas, above column-averaged mixing ratio of 100 ppm, there are enough isoprene molecules to saturate the atmosphere and render it opaque from the

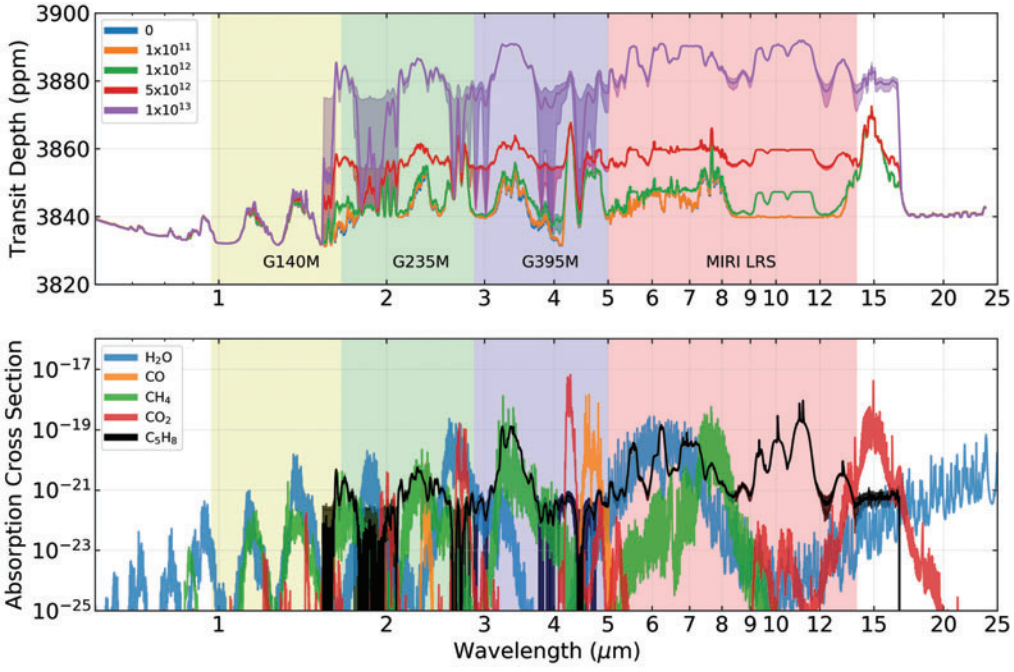

FIG. 11. Upper panel: Simulated spectra of exoplanets with H_2-dominated atmospheres transiting an M dwarf star for a range of isoprene surface fluxes from 0 to 1×10^{13} molecules/(cm^2 s). The *y*-axis shows transit depth (ppm), and the *x*-axis shows wavelength (μm). The spectra are simulated from 0.3 to 23 μm, covering the wavelength span of most of JWST's observation modes. The yellow, green, and blue region shows the spectral coverage of NIRSpec and the red region shows that of MIRI LRS. At low surface mixing ratios, the isoprene spectral features are not prominent as isoprene is mostly concentrated near the surface and rapidly decays as a function of altitude. Isoprene features are not noticeable until the surface flux is above 1×10^{11} molecules/(cm$^2\cdot$s). Above 1×10^{12} molecules/(cm$^2\cdot$s), increasing the surface flux of isoprene rapidly increases the amount of isoprene in the atmosphere and significantly increases the strength of isoprene's transmission spectral features. Lower panel: Comparison of isoprene cross-sections (Brauer *et al.*, 2014) with cross-sections of dominant molecules (except H_2, its absorption is mainly in the form of collision-induced absorption) in the atmosphere such as H_2O, CO, CH_4, and CO_2 (Gordon *et al.*, 2017). Color images are available online.

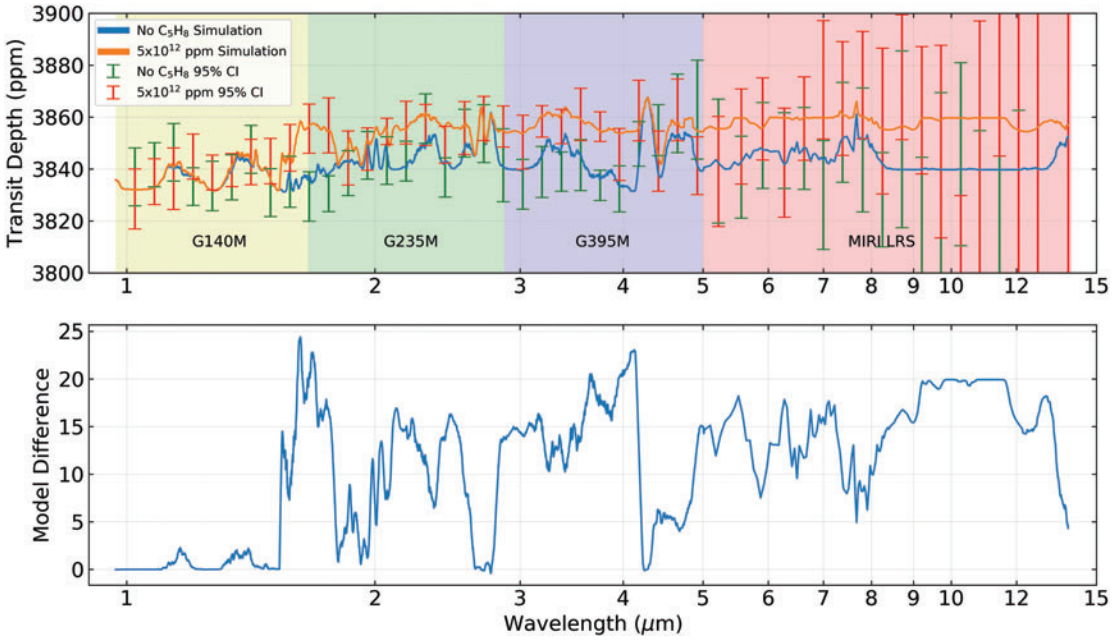

FIG. 12. Upper panel: Simulated H_2-dominated atmosphere observation using JWST for a 10 M_{Earth}, 1.75 R_{Earth} super-Earth transiting an M dwarf star given 20 transit observations per instrument (80 transits in total). The *y*-axis shows transit depth (ppm), and *x*-axis shows wavelength (μm). The simulated observation spans the wavelength range of the NIRSpec and MIRI instruments. We compare a model with no isoprene surface flux (blue line, green error-bar) and a model with 5×10^{12} molecules/($cm^2 \cdot s$) (orange line, red error-bar). The error bars are 95% confidence intervals for each model uniformly binned to a spectral resolution of $R = 10$. For this comparison, we take the isoprene cross-section as is and did not account for lab measurement error estimates. The error bar is attributed from observational noise only to more accurately reflect observation simulation. Lower panel: Difference between the two simulated spectra showing the spectral features of isoprene peaks. We show that within each instrument, there are more than more than 20 ppm transit depth differences between the two models; therefore, it is possible to achieve statistical significance and detect isoprene. Color images are available online.

surface to near or above the 0.01 bar level. Since the atmosphere is isothermal above 0.01 bar, the result is a featureless spectrum: a blackbody curve of much lower temperature than the surface temperature (Supplementary Appendix Fig. A2). Correction for this would require adapting the photochemistry model to use a self-consistent temperature-pressure profile, which is beyond the scope of this work.

4.2.3. Isoprene identification is hindered by methane. Detecting isoprene on an exoplanet atmosphere is challenging, requiring either very high isoprene production rate and/or long observation times. Another layer of challenge is that isoprene identification can be hindered by methane, unlike other biosignature gases we proposed: PH_3, which have distinguishable features around 4.5 μm (Sousa-Silva *et al.*, 2020), and NH_3, which have distinguishable features around 1.5, 2 μm (Huang, *et al.*, unpublished data). Therefore, we report on isoprene spectral distinguishability because, as observing capabilities improve in the future, the ultimate limiting factor for isoprene detection will remain the spectral strength, location, and distinguishability of its features, and these are immutable.

When compared with the expected major gases in habitable terrestrial planet atmospheres, isoprene broad band (*R* approximately 10–20) spectral features are distinguishable from molecules such as H_2O, CO_2, CO, NH_3, and H_2S (see Supplementary Appendix Fig. A3). However, distinguishing isoprene from CH_4 will be challenging and requires further discussion. The column-averaged mixing ratio of methane in the six simulation scenarios is in the range between 1 and 100 ppm (see Supplementary Appendix Fig. A1 for detailed mixing ratio profile). For H_2-dominated atmospheres, CH_4 should be readily present (Seager *et al.*, 2013). In CO_2-dominated atmospheres where CH_4 may not exist, isoprene contamination by CH_4 will not be an issue though other hydrocarbons might still confuse isoprene identification (see Section 5.2 for further discussion).

In an idealistic world with no observational constraints, the spectral features of all molecules are unique. Given the limitation of numbers of photons, however, instruments always have a finite spectral resolution. For detection of habitable exoplanet atmospheres, we must further trade spectral resolution in favor of increasing the (*SNR*) by binning the data after the data are obtained. We find that the data need to be binned to a relatively low spectra resolution of $R = 10$–20 to reach statistical significance (as demonstrated in Fig. 12).

At resolution lower than $R = 20$, distinguishing between isoprene spectral features and methane spectral features at shorter than 4 μm is not possible. Both methane and isoprene share the C-H stretch feature and its overtones; thus, if methane is present in significant quantities, the isoprene 1.6–1.7, 2.1–2.5, and 3.1–3.7 μm features will be masked by methane. In contrast, the 5.4–7.9 μm features and the 9–12 μm features do not overlap with methane spectral features (Fig. 13). Therefore, to confidently detect isoprene in H_2-dominated atmospheres,

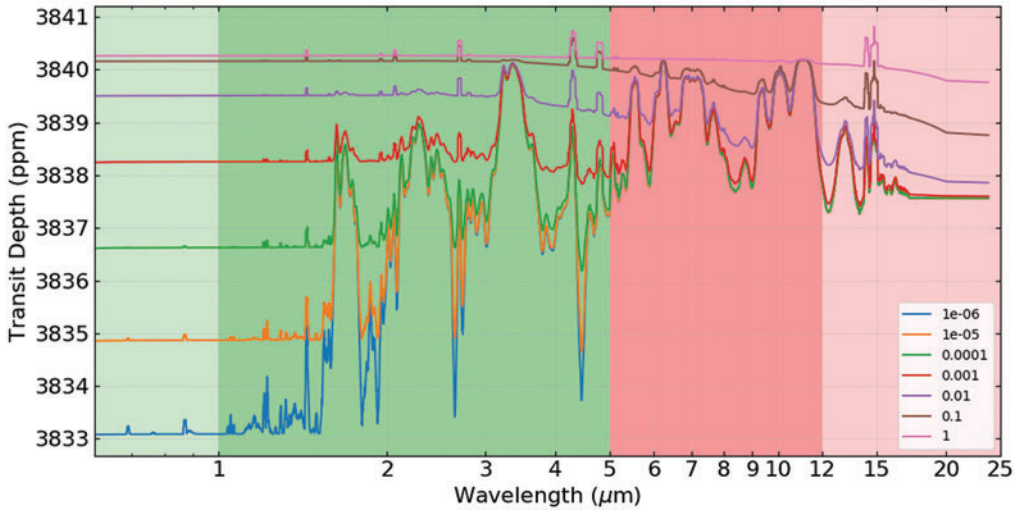

FIG. 13. Comparison of isoprene (orange) and methane (blue) cross-sections binned to $R = 20$. The axis shows cross-section ($cm^{-2} \cdot molecule^{-1}$) versus wavelength (μm). Cross-sections for isoprene are measured by Brauer *et al.* (2014). Cross-section for methane is calculated by using HITRAN line lists with standard pressure and temperature (Gordon *et al.*, 2017). The small panel shows a zoomed-in version of the isoprene-methane-shared spectral feature at 3.1–3.7 μm. We show that distinguishing between isoprene and methane spectral features at 3.1–3.7 μm is still possible at a spectral resolution of $R = 20$. Distinction between isoprene and methane at spectral resolution lower than this limit is not possible, and, therefore, detection of isoprene's 3.1–3.7 μm feature requires sufficient spectral resolution. We also show that isoprene's 5.4–7.5 μm features and the 9–12 μm features do not overlap with methane's spectral features, so detection of these two features can be done with a lower spectral resolution. Color images are available online.

the identification of both the 5.4–7.5 μm features and the 9–12 μm features is required, therefore requiring the use of both NIRSpec and MIRI, potentially more than doubling the number of transit observations required (since there are fewer photons at longer wavelengths).

4.3. Impact of haze on isoprene detection

We turn to an assessment of the detectability of isoprene in anoxic atmospheres with the presence of isoprene-induced haze. We find that haze will hinder but not completely mask the detection of isoprene unless the ratio between the total mass of isoprene-induced haze and the total mass of isoprene (haze-to-isoprene mass ratio) is above 10%. We consider a detection to be hindered if certain spectral features (in a confined wavelength range) are not detectable. We consider detection to be masked if no spectral features are detectable at any wavelength range. We simulate a wide range of scenarios to study how haze abundance, composition, size,[††] and size distribution can hinder isoprene detection.

Our models show that the most important factor that affects the detection of isoprene spectral features is the abundance of haze, followed by the size of the haze particles. The abundance of haze governs the overall opacity of the atmosphere, whereas the particle size plays a key role in determining the wavelength dependence of the opacity. Our simulations also suggest that the composition and the mean diameter of the haze particles matter less than the abundance and size distribution.

We quantify how different haze-to-isoprene mass ratios affect a simulated transmission spectrum (Fig. 14). We used our CO_2-dominated atmosphere archetype with an isoprene surface flux of 1×10^{13} molecules/($cm^2 \cdot s$) and other parameters described in Section 3. A sub-micron[‡‡] size particle's extinction cross-section at wavelengths longer than 3 μm decreases as the wavelength increases. The 1.6–1.7 and 2.1–2.5 μm features are sensitive to haze and can be diminished in strength for a haze-to-isoprene mass ratio of 0.0001. The 3.1–3.7 μm isoprene spectral feature is not affected for a haze-to-isoprene mass ratio of 0.0001 or lower but is masked for a ratio >0.001. The 5.4–7.5 μm spectral feature is not affected for a ratio of 0.001 or lower but is masked for a ratio >0.01. Finally, the 9–12 μm region is not affected for a ratio of 0.01 or lower but is masked for a ratio >0.1. Therefore, if the haze-to-isoprene mass ratio is 0.1 or less, detection of isoprene spectral features is still possible.

For context, the haze-to-methane mass ratio on Titan is ~0.1 at the thickest part of the haze layer at 400 km altitude. The number density of methane at the same altitude is 10^{12} molecule/cm^3 and the number density around 10^8 particles/cm^3 assuming the particles are 12.5 nm spheres (Fan *et al.* (2019) and using Titan tholin refractive indexes from the work of Khare *et al.* (1984). Although it is debatable whether habitable exoplanet atmospheres commonly attain the same abundance of haze as that of Titan, we adopt the haze-to-isoprene mass ratio of 0.1 as the upper bound.

Both experiments and models show that the mean radius of haze particles at standard temperature and pressure are 0.1 micron or smaller (He *et al.*, 2018; Hörst *et al.*, 2018), a

[††]In this work, we use size to mean the radius of the particle.

[‡‡]To reduce confusion, we use micron to denote particle radius and μm to denote spectral wavelength.

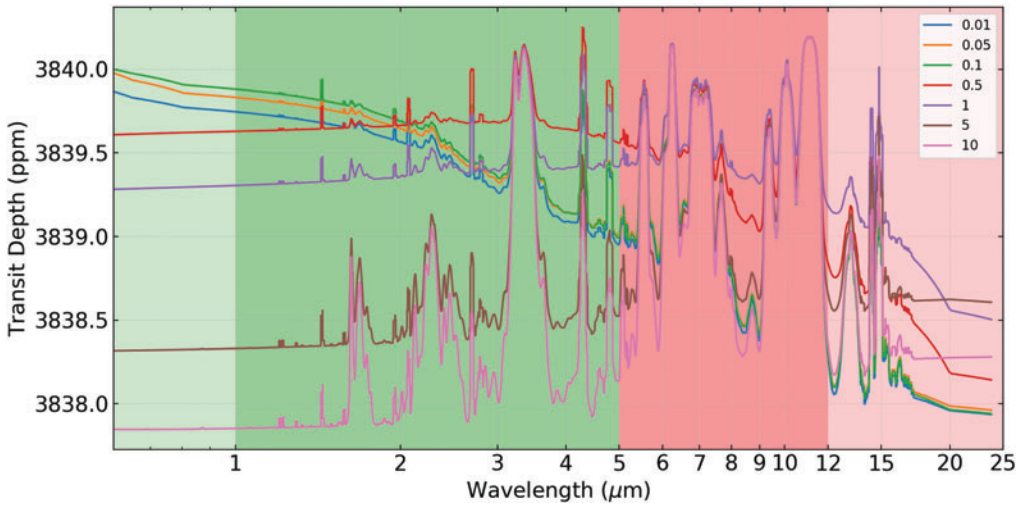

FIG. 14. Haze abundance effects on simulated transmission spectra demonstrated using a CO_2-dominated atmosphere with an isoprene surface flux of 1×10^{13} molecules/(cm$^2\cdot$s) for a habitable super Earth transiting an M dwarf star. The axes are transit depth (ppm) versus wavelength (μm). The isoprene-induced haze size distribution is a Gaussian distribution with mean of 89 nm and standard deviation of 25 nm, and it is approximated from the 10,000× metallicity, 300 K scenario as described in the work of Hörst *et al.* (2018). The refractive index proxy for isoprene is C_2H_2 (Dalzell and Sarofim, 1969). The different colored curves show the simulated transmission spectra as a function of haze/isoprene mass ratio from 1×10^{-6} to 1. Color images are available online.

particle size that affects shorter (*i.e.*, visible to near-infrared) rather than longer (*i.e.*, mid-infrared) wavelengths. This effect is well known from Mie theory, and it includes the point that once a particle radius is much smaller than the wavelength of light, scattering is in the Rayleigh regime and scales with wavelength as λ^{-4}. We study how different haze particle size affects simulated transmission spectra by using the same inputs as for the haze-to-mass ratio study depicted earlier and shown in Fig. 14. We set the haze-to-isoprene mass ratio to 0.01 and vary the mean particle radius from 0.01 to 10 microns.

For completeness, we explore the effect of mean particle size on the extinction cross-section for a size of 0.01–10 microns. We found that the haze extinction cross-section does not scale linearly with the size of the haze particles when assuming a fixed haze-to-isoprene mass ratio (total mass is constant). Taking Mie theory into account, the maximum strength for the extinction cross-section is for a mean particle size of 0.1 micron (for shorter wavelength) to 1.0 microns (for longer wavelength). For a haze particle size smaller than 0.1 micron, increasing the particle size increases the total extinction cross-section. Overall, different mean particle size will hinder or mask detection of different part of the spectra and is shown in more detail in Fig. 15.

Finally, we examine whether different types of refractive indices (as a proxy for haze particle composition) will

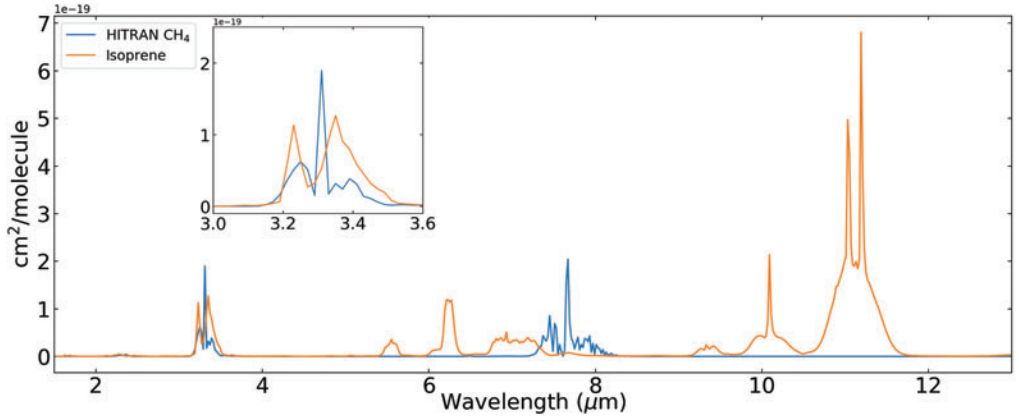

FIG. 15. Haze abundance effects on simulated transmission spectra demonstrated by using a CO_2-dominated atmosphere with an isoprene surface flux of 1×10^{13} molecules/(cm$^2\cdot$s) for a habitable super Earth transiting an M dwarf star. The haze/isoprene mass ratio of this simulation is set to 0.01, and the refractive index proxy for isoprene is C_2H_2 (Dalzell and Sarofim, 1969). The different colored curves show the simulated transmission spectra with varying haze mean particle size. Changes in the broad-band attenuation and spectral attenuation are not linear with an increase in the mean particle radius. Color images are available online.

impact detection. Based on the four types of materials we considered [Titan tholins (Khare *et al.*, 1984), HCN (Khare *et al.*, 1994), C_2H_2 (Dalzell and Sarofim, 1969), and octane (Anderson, 2000)], we found that although there are minor differences in wavelength-dependent opacities, none of these have unique absorption features that will hinder or mask isoprene spectral features.

4.4. Lack of isoprene false positives

On Earth, isoprene is exclusively produced by life (Section 2.2). Even so, one might suggest that isoprene could be formed geochemically, as a geological false positive, by reduction of carbon dioxide, by reduction of carbon monoxide, or by hydrogenation or dehydrogenation of hydrocarbons. However, the geochemical formation of isoprene on temperate, rocky planets is thermodynamically disfavored (Table 3). For any of the proposed isoprene formation reaction pathways, given the gas concentrations in terrestrial volcanoes, the calculated energy of formation of isoprene makes any geochemical formation scenario very unlikely (a positive Gibbs free energy (ΔG) means the reaction requires energy) (Table 3).

Molecules in a planetary atmosphere may potentially originate from several common abiotic sources, including: the interstellar medium (ISM); as leftover from planetary formation; meteorites and comets; photochemical processes in upper planetary atmospheres; and geological processes on planetary surfaces. None of these processes or environments can efficiently abiotically produce isoprene, as detailed later.

Isoprene and other hydrocarbons containing conjugated double bonds are not known to be a product of ISM chemistry (Ehrenfreund and Cami, 2010; McBride *et al.*, 2013) and are not identified among known ISM molecules (McElroy *et al.*, 2013). We note, however, that many other hydrocarbons, including unsaturated ones, have been detected in ISM (*e.g.*, CH, C_2H, CH_2, CH_3, CH_4, C_4H, C_5H, C_6H, C_6H_2, C_6H_6, as reviewed by McElroy *et al.*, 2013). Similarly, isoprene and other hydrocarbons containing conjugated double bonds are not detected in meteorites, including in the Murchison meteorite (Levy *et al.*, 1973; Sephton, 2004; Pizzarello and Shock, 2010), a meteorite famous for containing structurally diverse types of organic chemicals.

Photochemical processes in upper planetary atmospheres are also known to not produce isoprene.[§§] For example, isoprene and other complex hydrocarbons containing conjugated double bonds are not known to be produced in the atmosphere of Titan. Moreover, the simplest conjugated double bond hydrocarbon (1,3-butadiene) is also not likely to be formed abiotically. Limited theoretical work suggests that nonbiological production of 1,3-butadiene in Titan's atmosphere is, in principle, possible *via* photochemical reactions, although the rate of formation of 1,3-butadiene is predicted to be negligible. Indeed, so far 1,3-butadiene has not been detected on Titan (Newby *et al.*, 2007) and would likely condense onto haze given the low temperature of Titan. On the other hand, photochemical processes in Titan's atmosphere may lead to the formation of many unsaturated hydrocarbons (*e.g.*, C_2H_2, ethylene [C_2H_4], C_4H_2, C_6H_2, C_6H_6 etc.), none of which contain conjugated double bonds (Yung *et al.*, 1984; Maltagliati *et al.*, 2015).

Table 3. Proposed Geochemical Isoprene Formation Pathways and Energy of Formation of Isoprene from Plausible Geochemical Volatile Concentrations

Proposed geochemical isoprene formation pathways		ΔG *of reaction (kJ/mol)*
$5CO_2 + 14H_2$	$\rightarrow C_5H_8 + 10H_2O$	1670.1
$5CO + 9H_2$	$\rightarrow C_5H_8 + 5H_2O$	1294.8
$5CH_4$	$\rightarrow C_5H_8 + 6H_2$	477.7

ΔG is the free energy of reaction at 298 K assuming typical geochemical concentrations of H_2O, CO, CO_2, CH_4, and H_2 and 1 ppm isoprene. Average fractions of ''wet'' gas from magmatic and hydrothermal volcanic systems from the ASM database (Bains *et al.*, 2017): $H_2 = 0.0028$, $H_2O = 0.9223$, $CO = 0.000615$, $CO_2 = 0.05332$, $CH_4 = 4.206 \times 10^{-5}$. Nonbiological formation of isoprene from any terrestrial geological source is very unlikely for any of the proposed reaction pathways (positive ΔG).

C_5H_8 = isoprene.

The lack of chemical pathways leading to the abiotic formation of isoprene in a diverse host of planetary environments was recently strengthened by a series of photochemical laboratory experiments on the formation of various gases, including hydrocarbons. The exposure of various mixtures of basic gases such as H_2O, CO_2, CH_4, and NH_3 to UV light or plasma at various temperatures in simulated atmospheric scenarios did not show isoprene formation (nor any precursor hydrocarbons to isoprene's formation, nor any other conjugated dienes) (He *et al.*, 2019).

We conclude that isoprene has no known false positive sources. Consequently, its detection in an exoplanet atmosphere would be a strong indication of biological activity.

5. Discussion

We evaluated the candidacy of isoprene as a potential biosignature gas based on the principle that an ideal biosignature gas should satisfy all the following criteria: (1) is produced by life; (2) lacks abiotic false positives; (3) can accumulate to a detectable abundance in exoplanet atmospheres; and (4) has distinguishable spectral features. We have shown that isoprene satisfies the first two criteria (Sections 2 and 4). Isoprene satisfies the first and second criteria but can only satisfy the third and fourth criteria in some scenarios. Therefore, we consider isoprene as a good biosignature gas. Here, we discuss several factors limiting our analysis (Section 5.1), as well as the ability to distinguish isoprene from other hydrocarbons (Section 5.2). We end the discussion by exploring isoprene's ubiquity in many life-forms, and we introduce the concept of isoprene as a ''Biosphere Signature'' (Section 5.3).

5.1. Limitations of reference data

Our assessment of isoprene as a biosignature gas is constrained by the limited availability of spectral data, our

[§§]We note that on Earth a very small amount of isoprene is formed on the surface of Earth's oceans as a result of photodissociation of natural fatty acids (Ciuraru *et al.*, 2015). Such production, though not a result of direct biological action, is still an indirect result of biological activity and is, therefore, considered to be biological.

incomplete understanding of isoprene chemistry in anoxic atmospheres, and unknown but potential haze formation from isoprene in anoxic atmospheres. Here, we discuss these limitations and how they may affect our assessment.

5.1.1. Limitations with using absorption cross-sections from lab-measured spectra. Using cross-sections calculated from lab-measured data ''as is'' without estimating uncertainties for high isoprene mixing ratios can result in atmospheric spectra that are saturated and show artificially strong, wide, and featureless absorption bands (see Supplementary Appendix Fig. A4), which lead to inconclusive detection predictions. This effect is unphysical, because in some wavelength ranges, the true cross-section values are likely much smaller than the instrumental noise floor. The Brauer *et al.* (2014) wavelength-independent uncertainty is approximately four orders of magnitude weaker than the strongest absorption peaks of isoprene. Based on Beer-lambert law, for transmission spectroscopy, the cross-section uncertainty will also need to be eight orders of magnitude weaker than the strongest absorption peaks to avoid the unphysical effect. Therefore, we recommend future lab-based measurements of the isoprene cross-sections to focus on measuring the strength of the weak absorption features, or location of the spectra where there are no spectral peaks, so that it is possible to differentiate between real, but weak transitions and the noise floor.

A possible work-around method is to subtract the uncertainties from the data, leaving only the strongest peaks. However, we disfavor discarding cross-section values below an arbitrary value because it can remove weak, but real, absorption lines. Although individually these weak lines are negligible, collectively they can drastically change the overall opacity, and subsequently conclusions on the potential for detection. We show in Supplementary Appendix Fig. A4 how such an unphysical noise floor cut-off can artificially remove the weak features of isoprene and re-engineer the spectrum and associated detectability of isoprene.

In addition, we encourage the measurement of isoprene spectra to cover a broad temperature/pressure range relevant for exoplanet atmospheres. A broader coverage as compared with the current standard temperature and pressure measurements would allow extrapolation of isoprene cross-sections to conditions that are more appropriate for the upper atmosphere of a variety of exoplanets. Calculating molecular line lists by using *ab initio* theoretical quantum mechanical methods is computationally demanding (*e.g.*, Tennyson and Yurchenko, 2012), often requiring years of work even for a small molecule, and it is not currently possible to obtain accurate theoretical cross-sections for isoprene due to the complexity of the molecule (see Sousa-Silva *et al.*, 2019 for a more in-depth discussion on alternatives). However, we emphasize that our SEAS model is sufficiently versatile to be able to quickly update its predictions on isoprene detectability whenever improved cross-sections for isoprene become available.

5.1.2. Limitations to isoprene reaction rates. In this work, we have only focused on the reaction of isoprene with UV and the dominant radical species $O^{\bullet}$ and $^{\bullet}OH$. The photochemistry of isoprene with other, potentially relevant radicals, such as $H^{\bullet}$, $Cl^{\bullet}$, and $^{\bullet}C_nH_m$ is insufficiently studied. Inclusion of these radicals may potentially increase the isoprene destruction rate. Our models may not include all chemical reactions that are relevant to anoxic, temperate terrestrial planets. Therefore, more detailed studies of anoxic atmospheric chemical reaction networks are required.

Many M dwarf stars have frequent, strong flares. Flares introduce intense packets of UV radiation capable of destroying biosignature gases, including isoprene (Segura *et al.*, 2010; Tilley *et al.*, 2019). Recent work by Günther *et al.* (2019) has found 30% of late M dwarf stars and 5% of early M dwarf stars display active flaring events. Future photochemistry models, therefore, will require consideration of flaring activities and addressing how flaring activities impact habitability and accumulation of biosignature gases.

5.1.3. Limitations to understanding isoprene induced haze. No one has yet addressed the formation of isoprene-induced hazes in anoxic planetary atmospheres. On Earth, isoprene destruction rapidly leads to haze formation. Further studies on constraining the isoprene-haze mass ratio and mean particle size in anoxic planetary atmospheres are needed because sub-micron haze particles can heavily mute transmission spectral features at wavelengths up to 4 μm, as demonstrated in Section 4.3.

In addition, high-altitude hazes in an anoxic atmosphere could act as a UV shielding mechanism for biosignature gases, therefore increasing the probability of their accumulation (Segura *et al.*, 2005; Seager *et al.*, 2013).

5.2. Isoprene spectral distinguishability versus other hydrocarbons

In addition to isoprene and methane, all hydrocarbons have spectral features at 3.1–3.7 μm, due to the C-H bond stretching rovibrational band, and many have spectral features at 9–12 μm, due to the C-H bond bending rovibrational band. Figure 16 shows a comparison of isoprene with methane and other simple hydrocarbons that highlights the challenges in the unambiguous identification of isoprene. Though isoprene accounts for most of the non-methane hydrocarbons released by life on modern Earth (Sharkey *et al.*, 2008), simpler hydrocarbons have more favorable abiotic formation pathways, which may lead to their accumulation in the atmosphere. Therefore, we need to study isoprene distinguishability in the context of other hydrocarbons that may be readily present in the atmosphere.

The 3.1–3.7 μm features are the C-H bond stretching vibration features and can have three main functional groups: carbon single bonds (X-C-H) located at 3.45 μm, carbon double bonds (X=C-H) located at 3.23 μm, and carbon triple bonds (X#C-H) located at 3.03 μm (X denotes a non-hydrogen atom bonded to the carbon atom; see Section 3.1.2 for more details on these features). For molecules that have only one spectrally active functional group, distinguishing between molecules within each group requires a spectral resolution of at least $R=200$. Fortunately, isoprene has both the (X-C-H) bond and the (X=C-H) bond, so detection of its 3.1–3.7 μm can be done with a spectral resolution of $R=20$. We note, however, that a coincidental mixture of simple hydrocarbon molecules in the atmosphere can mimic the isoprene spectral features at 3.1–3.7 μm. For example, an equal amount of ethane (C_2H_6), which only contains the (X-C-H) bond, and C_2H_4,

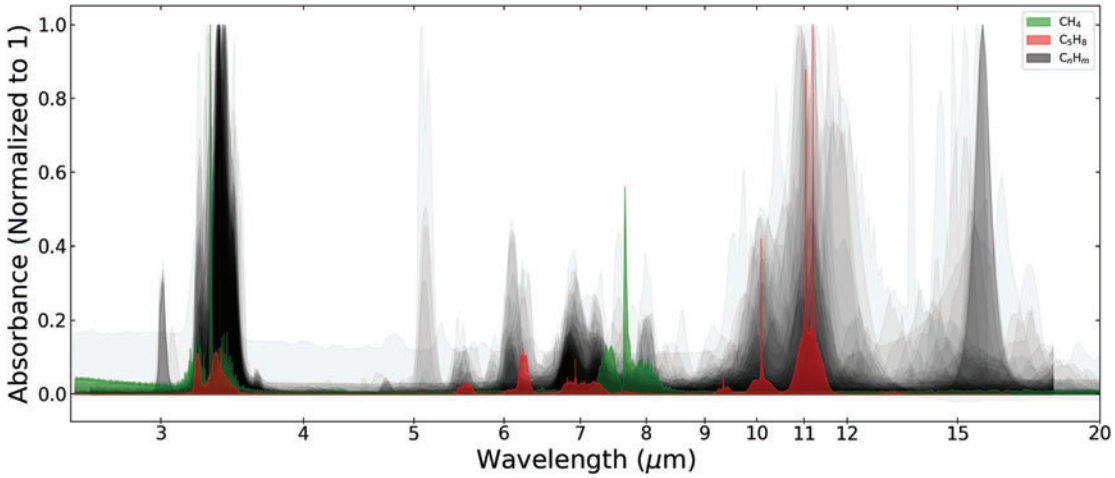

FIG. 16. Isoprene (red) and methane (green) versus 80 other hydrocarbon (grey) absorbances. The axes show absorbance (normalized to 1) versus wavelength (μm). The hydrocarbon absorbance data are taken from NIST lab-based measurements and include all hydrocarbons, with fewer than seven carbon atoms that have spectral measurements. Due to measurements being made with different instruments and experimental set-ups, we normalize the absorbances to one for a qualitative comparison. We show that although isoprene has many broad spectral features, it does not stand out when comparing with the collective sum of spectral features from other hydrocarbons. Therefore, it is possible for a coincidental combination of simple hydrocarbons to mimic isoprene spectral features. Color images are available online.

which contains only the (X=C-H) bond, would be indistinguishable from isoprene if observed at low resolutions. We additionally note that hydrocarbons containing the isoprene substructure can also mimic isoprene spectral features.

The isoprene spectral features at 9–12 μm are due to the vibrational bending of the C-H bond, and many contain many rovibrational substructures. Distinguishing isoprene from other hydrocarbon molecules in this spectral region can be challenging. Recent work by Sousa-Silva *et al.* (2019) developed a computational tool (RASCALL: Rapid Approximate Spectral Calculations for ALL) to estimate spectral data (position in the spectra and relative strength) for any molecule by combining functional group data from experimental measurements, organic chemistry, and quantum mechanics; these methods can aid in identifying which molecules struggle to be distinguished from one another, and they highlight the issues surrounding the distinguishability of isoprene from other hydrocarbons.

5.3. Isoprene as a "biosphere signature"

Isoprene stands out among the studied biosignature gases not only because it is produced in high abundance by life on the Earth but may also be due to isoprenoid biosynthetic pathways, which are responsible for synthesis of isoprene and many other terpenoids; these are present in virtually every domain of life on Earth, that is, Bacteria, Archaea, and Eukarya (see Section A2.2 in Supplementary Appendix A2). Although the synthesis and likely functions of isoprene on Earth are closely linked to oxygenic photosynthesis in plants, many non-photosynthesizing organisms make isoprene, and its synthesis is not dependent on an oxygenated atmosphere. It is plausible, therefore, to speculate that an entirely anaerobic biosphere could produce high levels of isoprene.

Even if isoprene itself is not made by every species on Earth, a wide variety of molecules that contain the isoprene-motif, or isoprenoids, are created. The isoprene motif and its structural derivatives are utilized to synthesize countless chemicals in all of Earth's life. In contrast to previously proposed classical type III biosignatures such as methyl chloride, methyl sulfide, and DMS, isoprenoids have a much larger coverage of the phylogenetic tree of life (Seager *et al.*, 2012).

Isoprenoids are produced by many evolutionary distant organisms occupying diverse ecological niches (*e.g.*, both marine and terrestrial surface and subsurface environments). Out of other proposed type III biosignature gases, only DMS is produced by a host of evolutionarily diverse organisms but nowhere near to the phylogenetic diversity of isoprenoid production. Other frequently cited type III biosignatures (such as N_2O and CH_3Cl) are produced by less diverse species. In addition, all of them inhabit very similar habitats (*e.g.*, methyl chloride is released mainly by several species of marine algae and to a lesser extent by the soil bacteria and fungi; 62% of the global N_2O emissions is produced by nitrifying and denitrifying bacteria and fungi in the soil; Maeda *et al.*, 2015). Isoprene and other isoprenoids do not have these limitations. Therefore, isoprene is the most widely made molecule, yet it is evaluated as a biosignature gas. Moreover, there are at least two distinct isoprenoid biosynthesis pathways, and isoprene synthesis likely has evolved independently multiple times so it is plausible to suggest that it might evolve in other worlds. Therefore, we postulate that isoprene and other volatile isoprenoids could be considered characteristic, unifying chemical signatures, specific and common to the whole Earth-type biosphere. In essence, isoprenoids are more than biosignatures—they are ''biosphere signatures''—chemicals that are a molecular fingerprint of the entire Earth-type biosphere.

Acknowledgments

The authors thank Mihkel Pajusalu, Karen Cady-Pereira, Robert Hargreaves, and Iouli Gordon, for lengthy discussions on using molecular absorption cross-sections calculated from

lab-measured spectra for exoplanet atmosphere simulations. They also thank Thomas Evans, Jason Eastman, Elisabeth Matthews, and the Seager group for helping them to establish the detection metric. Finally, they thank Joanna Petkowska for contributing Figs. 2 and 3.

Author Disclosure Statement

No competing financial interests exist.

Funding Information

The authors thank the MIT BOSE Fellow program, the Change Happens Foundation, the Heising-Simons Foundation, and NASA grants 80NSSC19K0471 and NNX15AC86G for partial funding of this work. S.R. gratefully acknowledges support from the Simons Foundation, grant number 495062.

Supplementary Appendices

Supplementary Appendix A1. Atmospheric Mixing Ratios and Temperature-Pressure Profiles

Supplementary Appendix Fig. A1

Supplementary Appendix Fig. A2

Supplementary Appendix Fig. A3

Supplementary Appendix Fig. A4

Supplementary Appendix A2. Structural Diversity and Biosynthesis of Isoprenoids

Supplementary Appendix Fig. A5

Supplementary Appendix Fig. A6

Supplementary Appendix Table A1

References

Abdelrahman OA, Park DS, Vinter KP, *et al.* (2017) Renewable isoprene by sequential hydrogenation of itaconic acid and dehydra-decyclization of 3-methyl-tetrahydrofuran. *ACS Catal* 7:1428–1431.

Allard F, Hauschildt PH, Alexander DR, *et al.* (1997) Model atmospheres of very low mass stars and brown dwarfs. *Annu Rev Astron Astrophys* 35:137–177.

Alvarez LA, Exton DA, Timmis KN, *et al.* (2009) Characterization of marine isoprene-degrading communities. *Environ Microbiol* 11:3280–3291.

Anderson MR (2000) Determination of infrared optical constants for single component hydrocarbon fuels. MS thesis, University of Missouri-Rolla, Parker Hall, Rolla, MO.

Arneth A, Monson RK, Schurgers G, *et al.* (2008) Why are estimates of global terrestrial isoprene emissions so similar (and why is this not so for monoterpenes)? *Atmos Chem Phys* 8:4605–4620.

Arney G, Domagal-Goldman SD, and Meadows VS (2018) Organic haze as a biosignature in anoxic Earth-like atmospheres. *Astrobiology* 18:311–329.

Bäck J, Aaltonen H, Hellén H, *et al.* (2010) Variable emissions of microbial volatile organic compounds (MVOCs) from root-associated fungi isolated from Scots pine. *Atmos Environ* 44:3651–3659.

Bagnasco G, Kolm M, Ferruit P, *et al.* (2007) Overview of the near-infrared spectrograph (NIRSpec) instrument on-board the James Webb Space Telescope (JWST). *International Society for Optics and Photonics*. https://doi.org/10.1117/12.735602

Bains W, Petkowski JJ, and Seager S (2017) Toward a list of molecules as potential biosignature gases for the search for life on exoplanets: thermodynamic profiling potential false positives. In *Astrobiology Science Conference (AbSciCon)*, Mesa, AZ. https://www.liebertpub.com/doi/pdf/10.1089/ast.2018.1954.

Batalha NE, Mandell A, Pontoppidan K, *et al.* (2017) PandExo: a community tool for transiting exoplanet science with JWST & HST. *Publ Astron Soc Pac* 129:064501.

Beck ZQ, Cervin MA, Chotani GK, *et al.* (2014) Recombinant anaerobic acetogenic bacteria for production of isoprene and/or industrial bio-products using synthesis gas. Google Patents, pp US 2014/0234926A1-US 2014/0234926A1.

Bentlage B, Rogers TS, Bachvaroff TR, *et al.* (2015) Complex ancestries of isoprenoid synthesis in dinoflagellates. *J Eukaryot Microbiol* 63:123–137.

Berenguer JA, Calderon V, Herce MD, *et al.* (1991) Spoilage of a bakery product (sobao pasiego) by isoprene-producing molds. *Rev Agroquim Tecnol Aliment* 31:580–583.

Berk A, Bernstein LS, Anderson GP, *et al.* (1998) MODTRAN cloud and multiple scattering upgrades with application to AVIRIS. *Remote Sens Environ* 65:367–375.

Bernath PF (2017) The atmospheric chemistry experiment (ACE). *J Quant Spectrosc Radiat Transf* 186:3–16.

Bernath PF, McElroy CT, Abrams MC, *et al.* (2005) Atmospheric chemistry experiment (ACE): mission overview. *Geophys Res Lett* 32:L15S01.

Brauer, C. S., Blake, T. A., Guenther, A. B., Sharpe, S. W., Sams, R. L., and Johnson, T. J.: Quantitative infrared absorption cross sections of isoprene for atmospheric measurements. *Atmos Meas Tech* 7, 3839–3847.

Chu PM, Guenther FR, Rhoderick GC, *et al.* (1999) The NIST quantitative infrared database. *J Res Natl Inst Stand Technol* 104:59.

Ciuraru R, Fine L, Pinxteren MV, *et al.* (2015) Unravelling new processes at interfaces: photochemical isoprene production at the sea surface. *Environ Sci Technol* 49:13199–13205.

Claeys M, Graham B, Vas G, *et al.* (2004) Formation of secondary organic aerosols through photooxidation of isoprene. *Science* 303:1173.

Cleveland CC and Yavitt JB (1998) Microbial consumption of atmospheric isoprene in a temperate forest soil. *Appl Environ Microbiol* 64:172–177.

Curdt W, Landi E, and Feldman U (2004) The SUMER spectral atlas of solar coronal features. *Astron Astrophys* 427:1045–1054.

Dal Corso J, Mietto P, Newton RJ, *et al.* (2012) Discovery of a major negative δ13C spike in the Carnian (Late Triassic) linked to the eruption of Wrangellia flood basalts. *Geology* 40:79–82.

Dalzell WH and Sarofim AF (1969) Optical constants of soot and their application to heat-flux calculations. *J Heat Transfer* 91:100–104.

Deneris ES, Stein RA, and Mead JF (1985) Acid-catalyzed formation of isoprene from a mevalonate-derived product using a rat liver cytosolic fraction. *J Biol Chem* 260:1382–1385.

Dillon TJ, Dulitz K, Groß C, *et al.* (2017) Temperature-dependent rate coefficients for the reactions of the hydroxyl radical with the atmospheric biogenics isoprene, alpha-pinene and delta-3-carene. *Atmos Chem Phys* 17:15137–15150.

Dlugokencky EJ, Nisbet EG, Fisher R, *et al.* (2011) Global atmospheric methane: budget, changes and dangers. *Philos Trans Royal Soc A Math Phys Eng Sci* 369:2058–2072.

Domagal-Goldman SD, Meadows VS, Claire MW, *et al.* (2011) Using biogenic sulfur gases as remotely detectable biosignatures on anoxic planets. *Astrobiology* 11:419–441.

Eastman RT, Buckner FS, Yokoyama K, *et al.* (2006) Thematic review series: lipid posttranslational modifications. Fighting parasitic disease by blocking protein farnesylation. *J Lipid Res* 47:233–240.

Ehrenfreund P and Cami J (2010) Cosmic carbon chemistry: from the interstellar medium to the early Earth. *Cold Spring Harb Perspect Biol* 2:a002097.

Exton DA, Suggett DJ, McGenity TJ, *et al.* (2013) Chlorophyll-normalized isoprene production in laboratory cultures of marine microalgae and implications for global models. *Limnol Oceanogr* 58:1301–1311.

Fall R and Copley SD (2000) Bacterial sources and sinks of isoprene, a reactive atmospheric hydrocarbon. *Environ Microbiol* 2:123–130.

Fall RR, Kuzma J, and Nemecek-Marshall M (1998) Materials and methods for the bacterial production of isoprene. Google Patents. US5849970A.

Fan J and Zhang R (2004) Atmospheric oxidation mechanism of isoprene. *Environ Chem* 1:140–149.

Fan S, Shemansky DE, Li C, *et al.* (2019) Retrieval of chemical abundances in Titan's upper atmosphere from Cassini UVIS observations with pointing motion. *Earth Space Sci* 6:1057–1066.

Firn R (2010) *Nature's Chemicals: The Natural Products that Shaped Our World*. Oxford University Press, Oxford, United Kingdom

France K, Froning CS, Linsky JL, *et al.* (2013) The ultraviolet radiation environment around M dwarf exoplanet host stars. *Astrophys J* 763:149.

Gardner JP, Mather JC, Clampin M, *et al.* (2006) The James Webb Space Telescope. *Space Sci Rev* 123:485–606.

Ge D, Xue Y, and Ma Y (2016) Two unexpected promiscuous activities of the iron–sulfur protein IspH in production of isoprene and isoamylene. *Microb Cell Fact* 15:79.

Gelmont D, Stein RA, and Mead JF (1981) Isoprene—the main hydrocarbon in human breath. *Biochem Biophys Res Commun* 99:1456–1460.

Gershenzon J (2008) Insects turn up their noses at sweating plants. *Proc Natl Acad Sci U S A* 105:17211–17212.

Gordon IE, Rothman LS, Hill C, *et al.* (2017) The HITRAN2016 molecular spectroscopic database. *J Quant Spectrosc Radiat Transf* 203:3–69.

Grauvogel C and Petersen J (2007) Isoprenoid biosynthesis authenticates the classification of the green alga *Mesostigma viride* as an ancient streptophyte. *Gene* 396:125–133.

Grenfell JL (2017) A review of exoplanetary biosignatures. *Phys Rep* 713:1–17.

Grenfell JL (2018) Atmospheric biosignatures. In *Handbook of Exoplanets*, edited by HJ Deeg and JA Belmontes, Springer International Publishing, Cham, pp 1–14.

Grochowski LL and White RH (2008) Promiscuous anaerobes. *Ann N Y Acad Sci* 1125:190–214.

Guenther A, Karl T, Harley P, *et al.* (2006) Estimates of global terrestrial isoprene emissions using MEGAN (Model of Emissions of Gases and Aerosols from Nature). *Atmos Chem Phys* 6:3181–3210.

Guenther AB, Jiang X, Heald CL, *et al.* (2012) The Model of Emissions of Gases and Aerosols from Nature version 2.1 (MEGAN2.1): an extended and updated framework for modeling biogenic emissions. *Geosci Model Dev* 5:1471–1492.

Günther MN, Zhan Z, Seager S, *et al.* (2019) Stellar flares from the first tess data release: exploring a new sample of M-dwarfs. *arXiv preprint* arXiv:1901.00443.

Harvey CM and Sharkey TD (2016) Exogenous isoprene modulates gene expression in unstressed *Arabidopsis thaliana* plants. *Plant Cell Environ* 39:1251–1263.

He C, Hörst SM, Lewis NK, *et al.* (2018) Laboratory simulations of haze formation in the atmospheres of super-Earths and mini-Neptunes: particle color and size distribution. *Astrophys J Lett* 856:L3.

He C, Hörst SM, Lewis NK, *et al.* (2019) Gas phase chemistry of cool exoplanet atmospheres: insight from laboratory simulations. *ACS Earth Space Chem* 3:39–50.

Hess BM, Xue J, Markillie LM, *et al.* (2013) Coregulation of terpenoid pathway genes and prediction of isoprene production in *Bacillus subtilis* using transcriptomics. *PLoS One* 8: e66104.

Hill C, Yurchenko SN, and Tennyson J (2013) Temperature-dependent molecular absorption cross sections for exoplanets and other atmospheres. *Icarus* 226:1673–1677.

Holland HD (2006) The oxygenation of the atmosphere and oceans. *Philos Trans Royal Soc B Biol Sci* 361:903–915.

Hörst SM, He C, Lewis NK, *et al.* (2018) Haze production rates in super-Earth and mini-Neptune atmosphere experiments. *Nat Astron* 2:303.

Hu R, Seager S, and Bains W (2012) Photochemistry in terrestrial exoplanet atmospheres. I. Photochemistry model and benchmark cases. *Astrophys J* 761:166.

Hughes R, Bernath P, and Boone C (2014) ACE infrared spectral atlases of the Earth's atmosphere. *J Quant Spectrosc Radiat Transf* 148:18–21.

Imlay L and Odom AR (2014) Isoprenoid metabolism in apicomplexan parasites. *Curr Clin Microbiol Rep* 1:37–50.

Jeans J (1930) *The Universe Around Us*. MacMillan Company. *Original from the University of California* 341.

Johns M, McCarthy P, Raybould K, *et al.* (2012) Giant Magellan telescope: overview. In *SPIE Astronomical Telescopes + Instrumentation, SPIE*. https://www.gmto.org/SPIE_2012/8444-52.pdf

Jones AMP, Shukla MR, Sherif SM, *et al.* (2016) Growth regulating properties of isoprene and isoprenoid-based essential oils. *Plant Cell Rep* 35:91–102.

Karl T, Potosnak M, Guenther A, *et al.* (2004) Exchange processes of volatile organic compounds above a tropical rain forest: implications for modeling tropospheric chemistry above dense vegetation. *J Geophys Res Atmos* 109:1–19.

Kasting JF (2014) Atmospheric composition of Hadean–early Archean Earth: the importance of CO. *Geol Soc Am Spl Papers* 504:19–28.

Kasting JF, Zahnle KJ, and Walker JCG (1983) Photochemistry of methane in the Earth's early atmosphere. *Precambrian Res* 20:121–148.

Kasting JF, Pollack JB, and Crisp D (1984) Effects of high CO_2 levels on surface temperature and atmospheric oxidation state of the early Earth. *J Atmos Chem* 1:403–428.

Kasting JF, Kopparapu R, Ramirez RM, *et al.* (2014) Remote life-detection criteria, habitable zone boundaries, and the frequency of Earth-like planets around M and late K stars. *Proc Natl Acad Sci U S A* 111:12641.

Kempton EMR, Lupu R, Owusu-Asare A, *et al.* (2017) Exo-Transmit: an open-source code for calculating transmission spectra for exoplanet atmospheres of varied composition. *Publ Astron Soc Pac* 129:044402.

Khare BN, Sagan C, Arakawa ET, *et al.* (1984) Optical constants of organic tholins produced in a simulated Titanian atmosphere: from soft X-ray to microwave frequencies. *Icarus* 60:127–137.

Khare BN, Sagan C, Thompson WR, *et al.* (1994) Optical properties of poly-HCN and their astronomical applications. *Can J Chem* 72:678–694.

Kiang NY, Domagal-Goldman S, Parenteau MN, *et al.* (2018) Exoplanet biosignatures: at the dawn of a new era of planetary observations. *Astrobiology* 18:619–629.

King J, Koc H, Unterkofler K, *et al.* (2010) Physiological modeling of isoprene dynamics in exhaled breath. *J Theor Biol* 267:626–637.

Knoll AH, Canfield DE, and Konhauser KO (2012) *Fundamentals of Geobiology*. John Wiley & Sons, Hoboken, NJ.

Kochanov RV, Gordon IE, Rothman LS, *et al.* (2016) HITRAN Application Programming Interface (HAPI): a comprehensive approach to working with spectroscopic data. *J Quant Spectrosc Radiat Transf* 177:15–30.

Köksal M, Zimmer I, Schnitzler J-P, *et al.* (2010) Structure of isoprene synthase illuminates the chemical mechanism of teragram atmospheric carbon emission. *J Mol Biol* 402:363–373.

Korhonen H, Carslaw KS, Spracklen DV, *et al.* (2008) Influence of oceanic dimethyl sulfide emissions on cloud condensation nuclei concentrations and seasonality over the remote Southern Hemisphere oceans: a global model study. *J Geophys Res Atmos* 113, D15204, https://doi.org/10.1029/2007JD009718.

Kuzma J, Nemecek-Marshall M, Pollock WH, *et al.* (1995) Bacteria produce the volatile hydrocarbon isoprene. *Curr Microbiol* 30:97–103.

Kuzuyama T and Seto H (2012) Two distinct pathways for essential metabolic precursors for isoprenoid biosynthesis. *Proc Jpn Acad Ser B Phys Biol Sci* 88:41–52.

Laothawornkitkul J, Paul ND, Vickers CE, *et al.* (2008) Isoprene emissions influence herbivore feeding decisions. *Plant Cell Environ* 31:1410–1415.

Levy RL, Grayson MA, and Wolf CJ (1973) The organic analysis of the murchison meteorite. *Geochim Cosmochim Acta* 37:467–483.

Linstrom PJ and Mallard WG (2001) The NIST Chemistry WebBook: a chemical data resource on the internet. *J Chem Eng Data* 46:1059–1063.

Loferer-Krößbacher M, Klima J, and Psenner R (1998) Determination of bacterial cell dry mass by transmission electron microscopy and densitometric image analysis. *Appl Environ Microbiol* 64:688–694.

Logan BA, Monson RK, and Potosnak MJ (2000) Biochemistry and physiology of foliar isoprene production. *Trends Plant Sci* 5:477–481.

Lohr M, Schwender J, and Polle JEW (2012) Isoprenoid biosynthesis in eukaryotic phototrophs: a spotlight on algae. *Plant Sci* 185–186:9–22.

Ludwiczuk A, Skalicka-Woźniak K, and Georgiev MI (2017) Terpenoids. In *Pharmacognosy*, Badal S and Delgoda R (eds) pp 233–266. https://doi.org/10.1016/B978-0-12-802104-0.00011-1.

Maeda K, Spor A, Edel-Hermann V, *et al.* (2015) N(2)O production, a widespread trait in fungi. *Sci Rep* 5:9697.

Maltagliati L, Bézard B, Vinatier S, *et al.* (2015) Titan's atmosphere as observed by Cassini/VIMS solar occultations: CH_4, CO and evidence for C_2H_6 absorption. *Icarus* 248: 1–24.

McBride EJ, Millar TJ, and Kohanoff JJ (2013) Organic synthesis in the interstellar medium by low-energy carbon irradiation. *J Phys Chem A* 117:9666–9672.

McElroy D, Walsh C, Markwick AJ, *et al.* (2013) The UMIST database for astrochemistry 2012. *Astron Astrophys* 550:A36.

McFiggans G, Mentel TF, Wildt J, *et al.* (2019) Secondary organic aerosol reduced by mixture of atmospheric vapours. *Nature* 565:587–593.

McGenity TJ, Crombie AT, and Murrell JC (2018) Microbial cycling of isoprene, the most abundantly produced biological volatile organic compound on Earth. *ISME J* 12:931–941.

Michelozzi M, Raschi A, Tognetti R, *et al.* (1997) Eco-ethological analysis of the interaction between isoprene and the behaviour of Collembola. *Pedobiologia* 41:210–214.

Miller-Ricci E, Meyer MR, Seager S, *et al.* (2009) On the emergent spectra of hot protoplanet collision afterglows. *Astrophys J* 704:770.

Moore RM, Oram DE, and Penkett SA (1994) Production of isoprene by marine phytoplankton cultures. *Geophys Res Lett* 21:2507–2510.

Murakami M, Shibuya K, Nakayama T, *et al.* (2007) Geranylgeranyl reductase involved in the biosynthesis of archaeal membrane lipids in the hyperthermophilic archaeon *Archaeoglobus fulgidus*. *FEBS J* 274:805–814.

Murphy N, Roswitha B, Weber KA, *et al.* (2017) Production of isoprene by methane-producing archaea. Google Patents. US20170175145A1.

Newby JJ, Stearns JA, Liu C-P, *et al.* (2007) Photochemical and discharge-driven pathways to aromatic products from 1,3-butadiene. *J Phys Chem A* 111:10914–10927.

Panchenko YN and De Maré GR (2008) Vibrational analysis of buta-1, 3-diene and its deutero and 13 C derivatives and some of their rotational isomers. *J Struct Chem* 49:235.

Pascale E, Bezawada N, Barstow J, *et al.* (2018) The ARIEL space mission. Space Telescopes and Instrumentation 2018: optical, Infrared, and Millimeter Wave. In *International Society for Optics and Photonics* 106980H:10.

Paulson SE, Flagan RC, and Seinfeld JH (1992) Atmospheric photooxidation of isoprene part I: the hydroxyl radical and ground state atomic oxygen reactions. *Int J Chem Kinet* 24: 79–101.

Peñuelas J, Llusia J, Asensio D, *et al.* (2005) Linking isoprene with plant thermotolerance, antioxidants and monoterpene emissions. *Plant Cell Environ* 28:278–286.

Pérez-Gil J and Rodríguez-Concepción M (2013) Metabolic plasticity for isoprenoid biosynthesis in bacteria. *Biochem J* 452:19–25.

Pilcher CB (2003) Biosignatures of early Earths. *Astrobiology* 3:471–486.

Pizzarello S and Shock E (2010) The organic composition of carbonaceous meteorites: the evolutionary story ahead of biochemistry. *Cold Spring Harb Perspect Biol* 2: a002105.

Rackham BV, Apai D, and Giampapa MS (2018) The transit light source effect: false spectral features and incorrect densities for M-dwarf transiting planets. *Astrophys J* 853: 122.

Rohmer M (1999) The discovery of a mevalonate-independent pathway for isoprenoid biosynthesis in bacteria, algae and higher plants. *Nat Prod Rep* 16:565–574.

Rohmer M (2010) Methylerythritol phosphate pathway. In *Comprehensive Natural Products II*, Mander L and Liu H-W (eds) Elsevier Science: pp 517–555.

Rothman LS, Gordon IE, Barber RJ, *et al.* (2010) HITEMP, the high-temperature molecular spectroscopic database. *J Quant Spectrosc Radiat Transf* 111:2139–2150.

Royer DL, Berner RA, Montañez IP, *et al.* (2004) CO_2 as a primary driver of phanerozoic climate. *GSA Today* 14:4–10.

Schöller C, Molin S, and Wilkins K (1997) Volatile metabolites from some gram-negative bacteria. *Chemosphere* 35:1487–1495.
Schöller CEG, Gürtler H, Pedersen R, *et al.* (2002) Volatile metabolites from actinomycetes. *J Agric Food Chem* 50: 2615–2621.
Schreier F, Städt S, Hedelt P, *et al.* (2018) Transmission spectroscopy with the ACE-FTS infrared spectral atlas of Earth: a model validation and feasibility study. *Mol Astrophys* 11:1–22.
Schwieterman EW, Kiang NY, Parenteau MN, *et al.* (2018) Exoplanet biosignatures: a review of remotely detectable signs of life. *Astrobiology* 18:663–708.
Seager S (2010) *Exoplanet Atmospheres: Physical Processes*, Princeton University Press, Princeton, NJ.
Seager S, Bains W, and Hu R (2013) Biosignature gases in H_2-dominated atmospheres on rocky exoplanets. *Astrophys J* 777:95.
Seager S, Bains W, and Petkowski JJ (2016) Toward a list of molecules as potential biosignature gases for the search for life on exoplanets and applications to terrestrial biochemistry. *Astrobiology* 16:465–485.
Seager S, Huang J, Petkowski JJ, *et al.* (2020) Laboratory studies on the viability of life in H_2-dominated exoplanet atmospheres. *Nat Astron* 4:802–806.
Seager S, Schrenk M, and Bains W (2012) An astrophysical view of Earth-based metabolic biosignature gases. *Astrobiology* 12:61–82.
Segura A, Kasting JF, Meadows V, *et al.* (2005) Biosignatures from Earth-like planets around M dwarfs. *Astrobiology* 5:706–725.
Segura A, Walkowicz LM, Meadows V, *et al.* (2010) The effect of a strong stellar flare on the atmospheric chemistry of an Earth-like planet orbiting an M dwarf. *Astrobiology* 10:751–771.
Seinfeld JH and Pandis SN (2016) *Atmospheric Chemistry and Physics: From Air Pollution to Climate Change*, John Wiley & Sons, Hoboken, NJ.
Sephton MA (2004) Organic matter in ancient meteorites. *Astron Geophys* 45:2.08–2.14.
Sharkey TD (1996) Isoprene synthesis by plants and animals. *Endeavour* 20:74–78.
Sharkey TD and Loreto F (1993) Water stress, temperature, and light effects on the capacity for isoprene emission and photosynthesis of kudzu leaves. *Oecologia* 95:328–333.
Sharkey TD and Monson RK (2017) Isoprene research—60 years later, the biology is still enigmatic. *Plant Cell Environ* 40:1671–1678.
Sharkey TD, Wiberley AE, and Donohue AR (2008) Isoprene emission from plants: why and how. *Ann Bot* 101:5–18.
Shennan JL (2005) Utilisation of C_2–C_4 gaseous hydrocarbons and isoprene by microorganisms. *J Chem Technol Biotechnol* 81:237–256.
Sivy TL, Shirk MC, and Fall R (2002) Isoprene synthase activity parallels fluctuations of isoprene release during growth of *Bacillus subtilis*. *Biochem Biophys Res Commun* 294:71–75.
Skidmore W, TMT International Science Development Teams, and TMT Science Advisory Committee (2015) Thirty meter telescope detailed science case: 2015. *Res Astron Astrophy* 15:1945.
Sousa-Silva C, Al-Refaie AF, Tennyson J, *et al.* (2015) ExoMol line lists—VII. The rotation–vibration spectrum of phosphine up to 1500K. *Mon Notices Royal Astron Soc* 446:2337–2347.
Sousa-Silva C, Petkowski JJ, and Seager S (2019) Molecular simulations for the spectroscopic detection of atmospheric gases. *Phys Chem Chem Phys* 21:18970–18987.
Sousa-Silva C, Seager S, Ranjan S, *et al.* (2020) Phosphine as a biosignature gas in exoplanet atmospheres. *Astrobiology* 20: 235–268.
Takagi S, Mahieux A, Wilquet V, *et al.* (2019) An uppermost haze layer above 100 km found over Venus by the SOIR instrument onboard Venus Express. *Earth Planets Space* 71:124.
Tamai R and Spyromilio J (2014) European extremely large telescope: progress report. *Proc. SPIE 9145, Ground-based and Airborne Telescopes V,* 91451E (22 July 2014); https://doi.org/10.1117/12.2058467.
Taylor TC, Smith MN, Slot M, *et al.* (2019) The capacity to emit isoprene differentiates the photosynthetic temperature responses of tropical plant species. *Plant Cell Environ* 42: 2448–2457.
Teng AP, Crounse JD, and Wennberg PO (2017) Isoprene peroxy radical dynamics. *J Am Chem Soc* 139:5367–5377.
Tennyson J and Yurchenko SN (2012) ExoMol: molecular line lists for exoplanet and other atmospheres. *Mon Notices Royal Astron Soc* 425:21–33.
Tennyson J, Yurchenko SN, Al-Refaie AF, *et al.* (2016) The ExoMol database: molecular line lists for exoplanet and other hot atmospheres. *J Mol Spectrosc* 327:73–94.
Tessenyi M, Tinetti G, Savini G, *et al.* (2013) Molecular detectability in exoplanetary emission spectra. *Icarus* 226:1654–1672.
Tian H, Chen G, Lu C, *et al.* (2015) Global methane and nitrous oxide emissions from terrestrial ecosystems due to multiple environmental changes. *Ecosyst Health Sustain* 1:1–20.
Tilley MA, Segura A, Meadows V, *et al.* (2019) Modeling repeated M dwarf flaring at an Earth-like planet in the habitable zone: atmospheric effects for an unmagnetized planet. *Astrobiology* 19:64–86.
Velikova V, Sharkey TD, and Loreto F (2012) Stabilization of thylakoid membranes in isoprene-emitting plants reduces formation of reactive oxygen species. *Plant Signal Behav* 7: 139–141.
Vickers CE, Gershenzon J, Lerdau MT, and Loreto F (2009) A unified mechanism of action for volatile isoprenoids in plant abiotic stress. *Nat Chem Biol* 5:283–291.
Wagner WP, Nemecek-Marshall M, and Fall R (1999) Three distinct phases of isoprene formation during growth and sporulation of *Bacillus subtilis*. *J Bacteriol* 181:4700–4703.
Wiemer AJ, Wiemer RJH, and David F (2009) The intermediate enzymes of isoprenoid metabolism as anticancer targets. *Anticancer Agents Med Chem* 9:526–542.
Wiscombe WJ (1979) Mie scattering calculations; advances in technique and fast, vector-speed computer codes, National Technical Reports Library, US Department of Commerce. NTIS Issue Number 197926.
Wright GS, Rieke G, Boeker T, *et al.* (2010) Progress with the design and development of MIRI, the mid-IR instrument for JWST. *Proc. SPIE 7731, Space Telescopes and Instrumentation 2010: Optical, Infrared, and Millimeter Wave,* 77310E:10 (4 August 2010); doi: 10.1117/12.857262
Xue J and Ahring BK (2011) Enhancing isoprene production by genetic modification of the 1-deoxy-d-xylulose-5-phosphate pathway in *Bacillus subtilis*. *Appl Environ Microbiol* 77: 2399–2405.
Yokouchi Y, Takenaka A, Miyazaki Y, *et al.* (2015) Emission of methyl chloride from a fern growing in subtropical, temperate, and cool-temperate climate zones. *J Geophys Res Biogeosci* 120:1142–1149.
Yung YL, Allen M, and Pinto JP (1984) Photochemistry of the atmosphere of Titan: comparison between model and observations. *Astrophys J Suppl Ser* 55:465–506.
Yurchenko SN and Tennyson J (2014) ExoMol line lists—IV. The rotation–vibration spectrum of methane up to 1500K. *Mon Notices Royal Astron Soc* 440:1649–1661.

Yurchenko SN, Barber RJ, and Tennyson J (2011) A variationally computed line list for hot NH3. *Mon Notices Royal Astron Soc* 413:1828–1834.

Yurchenko SN, Al-Refaie AF, and Tennyson J (2018) ExoCross: a general program for generating spectra from molecular line lists. *Astron Astrophys* 614:A131.

Zahnle KJ (1986) Photochemistry of methane and the formation of hydrocyanic acid (HCN) in the Earth's early atmosphere. *J Geophys Res Atmos* 91:2819–2834.

Zhang R, Suh I, Lei W, *et al.* (2000) Kinetic studies of OH-initiated reactions of isoprene. *J Geophys Res Atmos* 105: 24627–24635.

Zhang X, Strobel DF, and Imanaka H (2017) Haze heats Pluto's atmosphere yet explains its cold temperature. *Nature* 551:352–355.

Zuo Z, Weraduwage SM, Lantz AT, *et al.* (2019) Isoprene acts as a signaling molecule in gene networks important for stress responses and plant growth. *Plant Physiol* 180:124–152.

Address correspondence to:
Zhuchang Zhan
Department of Earth, Atmospheric, and Planetary Sciences
MIT
77 Massachusetts Ave
Cambridge, MA 02139
USA
E-mail: zzhan@mit.edu

Submitted 24 July 2019
Accepted 16 January 2021

Abbreviations Used

C_2H_4 = ethylene
C_2H_6 = ethane
C_5H_8 = isoprene
CH_3Cl = methyl chloride
CH_4 = methane
DMAPP = dimethylallyl pyrophosphate
DMS = dimethyl sulfide
IPP = isopentenyl pyrophosphate
IR = infrared
ISM = interstellar medium
JWST = James Webb Space Telescope
MEP = methylerythritol phosphate
MVA = mevalonate
N_2O = nitrous oxide
PH_3 = phosphine
ppbv = parts per billion
SEAS = Simulated Exoplanet Atmosphere Spectra
UV = ultraviolet
UV-Vis = ultraviolet-visible